

# Inverse Reinforcement Learning via Nonparametric Spatio-Temporal Subgoal Modeling

**Adrian Šošić**

**Abdelhak M. Zoubir**

*Signal Processing Group*

*Technische Universität Darmstadt*

*64283 Darmstadt, Germany*

ADRIAN.SOSIC@SPG.TU-DARMSTADT.DE

ZOUBIR@SPG.TU-DARMSTADT.DE

**Elmar Rueckert**

*Institute for Robotics and Cognitive Systems*

*University of Lübeck*

*23538 Lübeck, Germany*

RUECKERT@ROB.UNI-LUEBECK.DE

**Jan Peters**

*Autonomous Systems Labs*

*Technische Universität Darmstadt*

*64289 Darmstadt, Germany*

MAIL@JAN-PETERS.NET

**Heinz Koepl**

*Bioinspired Communication Systems*

*Technische Universität Darmstadt*

*64283 Darmstadt, Germany*

HEINZ.KOEPPL@BCS.TU-DARMSTADT.DE

**Editor:**

## Abstract

Recent advances in the field of inverse reinforcement learning (IRL) have yielded sophisticated frameworks which relax the original modeling assumption that the behavior of an observed agent reflects only a single intention. Instead, the demonstration data is typically divided into parts, to account for the fact that different trajectories may correspond to different intentions, e.g., because they were generated by different domain experts. In this work, we go one step further: using the intuitive concept of *subgoals*, we build upon the premise that even a single trajectory can be explained more efficiently *locally* within a certain context than globally, enabling a more compact representation of the observed behavior. Based on this assumption, we build an implicit intentional model of the agent's goals to forecast its behavior in unobserved situations. The result is an integrated Bayesian prediction framework which provides smooth policy estimates that are consistent with the expert's plan and significantly outperform existing IRL solutions. Most notably, our framework naturally handles situations where the intentions of the agent change with time and classical IRL algorithms fail. In addition, due to its probabilistic nature, the model can be straightforwardly applied in an active learning setting to guide the demonstration process of the expert.

**Keywords:** Learning from Demonstration, Inverse Reinforcement Learning, Bayesian Nonparametric Modeling, Subgoal Inference, Graphical Models, Gibbs Sampling

## 1. Introduction

Inverse reinforcement learning (IRL) refers to the problem of inferring the intention of an agent, called *the expert*, from observed behavior. Under the Markov decision process (MDP) formalism (Sutton and Barto, 1998), this intention is encoded in form of a reward function, which provides the agent with instantaneous feedback for each situation that is encountered during the decision-making process. While classical IRL methods such as (Ng and Russell, 2000; Abbeel and Ng, 2004; Ziebart et al., 2008; Ramachandran and Amir, 2007; Levine et al., 2011) assume a single *global* reward model to explain the entire demonstration data set, recent methods relax this modeling assumption by allowing the intention of the agent to change with time (Nguyen et al., 2015), or by hypothesizing that the data set is inherently composed of several parts (Dimitrakakis and Rothkopf, 2011), where different trajectories reflect the intentions of different experts.

In this work, we go a step further and start from the premise that, even in the case of a single expert or trajectory, the demonstrated behavior can be explained more efficiently *locally* within a certain context than by a single global reward model. As an illustrative example, consider the task shown in Figure 10a, where the expert approaches a set of intermediate goal positions before finally heading toward a global goal state. Despite the simplicity of the task, the encoding of such a behavior in a global intention model requires a reward structure that comprises a comparably large number of redundant state-action based rewards. Alternative solution strategies include task-dependent expansions of the agent’s state representation, e.g., to memorize the last visited goal (Krishnan et al., 2016), or they resort to more general decision-making frameworks like semi-MDPs/options (Bradtke and Duff, 1994; Sutton et al., 1999) in order to achieve the necessary level of abstraction.

By contrast, the method presented in this paper learns a rather simple task representation based on the intuitive concept of *subgoals*, which allows to efficiently encode the expert behavior using task-appropriate partitionings of the state space/the data set. Our framework builds upon the method of Bayesian nonparametric inverse reinforcement learning (BNIRL, Michini and How, 2012), which can be used to build a subgoal representation of a task from demonstration data—however, without learning the underlying subgoal relationships or constructing a policy model that can predict the actions of the demonstrator. In order to address this limitation, we generalize the BNIRL model, using insights from our previous works on nonparametric subgoal modeling (Šošić et al., 2018a) and policy recognition (Šošić et al., 2018b), to explicitly describe the local dependencies between the expert demonstrations and the underlying subgoal structure, which allows us to build a compact intentional model of the expert’s behavior. The result is an integrated Bayesian prediction framework which exploits the spatio-temporal context of the demonstrations and is capable of producing smooth policy estimates that are consistent with the expert’s plan. Capturing the full posterior information of the data set further enables us to apply the proposed approach in an active learning setting, where the data acquisition process is controlled by the posterior predictive distribution of our model.

In our experimental study, we compare the proposed approach with common baseline methods on a variety of benchmark and real-world scenarios. The results reveal that our approach performs significantly better than the original BNIRL model and alternative IRL solutions on all considered tasks. Interestingly enough, our algorithm outperforms the

baselines even when the expert’s true reward structure is dense and the underlying subgoal assumption is violated.

## 1.1 Related Work

The idea of decomposing complex behavior into smaller parts has been around for long and researchers have approached the problem in many different ways. While the overall field of methods is too large to be covered here, most existing approaches can be clearly categorized according to certain criteria. First of all, methods differ in their exact problem formulation, i.e., one can distinguish between *active* methods, where the learning algorithm can freely interact with the environment (e.g., hierarchical reinforcement learning, Botvinick, 2012; Al-Emran, 2015), and *passive* methods, where the behavioral model is trained solely through observation (learning from demonstration, Argall et al., 2009). Second, one can discriminate between methods that build an intentional model of the considered task (IRL and option-based models, Choi and Kim, 2012; Sutton et al., 1999), and such that work directly on the control/trajectory level (skill learning, movement primitives, Konidaris et al., 2012; Schaal et al., 2005). The latter distinction is sometimes referred to as *intentional/subintentional* methods (Albrecht and Stone, 2017; Panella and Gmytrasiewicz, 2017). In order to give a concise summary of the work that is most relevant to ours, we restrict ourselves to demonstration-based approaches, with a focus on intentional methods, the field of which is considerably smaller. For an overview of reinforcement learning based methods, we refer to existing literature, e.g., the work by Daniel et al. (2016).

First, there are the methods that pursue a decomposition of the observed behavior on the global level, using trajectory-based IRL approaches. For example, Dimitrakakis and Rothkopf (2011) proposed a hierarchical prior over reward functions to account for the fact that different trajectories in the data set could reflect different behavioral intentions, e.g., because they were generated by different domain experts. Similarly, Babeş-Vroman et al. (2011) follow an expectation-maximization based clustering approach to group individual trajectories according to their underlying reward functions. Choi and Kim (2012) generalized this idea by proposing a nonparametric Bayesian model in which the number of intentions is a priori unbounded.

While these methods consider the demonstration data on a global scale, our work is concerned with the problem of *subgoal modeling*, which is often conducted in the form of option-based reasoning (Sutton et al., 1999). For instance, Tamassia et al. (2015) proposed a clustering approach based on state distances to find a minimal set of options that explain the expert behavior. While the method provides a simple alternative to hand-crafting options, it does not allow for a probabilistic treatment of the data and involves many ad-hoc design choices. Going in the same direction, Daniel et al. (2016) presented a more principled, probabilistic option framework based on expectation-maximization. The framework is not only capable of automatically inferring sub-policies from trajectory information, it can be also used in a reinforcement learning setting for intra-option learning. However, the resulting behavioral model is based only on point estimates of the policy parameters and the number of sub-policies needs to be specified manually. The latter problem is solved by Krishnan et al. (2016), who proposed a hierarchical nonparametric IRL framework to learn a sequential representation of the demonstrated task, based on a set of transition regions

that are defined through local changes in linearity of the observed behavior. However, in contrast to the work by Daniel et al. (2016), inference is not performed jointly but in several isolated stages where, again, each stage only propagates a point estimate of the associated model parameters. Moreover, the temporal relationship of the demonstration data, used to identify the local linearity changes, is considered only in an ad-hoc fashion through the use of a windowing function.

Another general class of models, which explicitly addresses this issue, employs a hidden Markov model (HMM) structure to establish a temporal relationship between the demonstrations. For instance, the work presented by Nguyen et al. (2015) can be regarded as a generalization of the model by Babeş-Vroman et al. (2011), extending their expectation-maximization framework by imposing a Markov structure on the reward model. Similarly, Niekum et al. (2012) use an extended HMM to segment the demonstrations into vector autoregressive models, in order to learn a suitable set of movement primitives. However, the learning of those primitives is done in a post-processing step, meaning that the quality of the final representation crucially depends on the success of the initial segmentation stage. In contrast, the method by Rueckert et al. (2013) automatically learns the position and timing of multiple subgoals in the form of via-points, but the number of these points is assumed to be known and the system objective is encoded in a global cost function. Recently, Lioutikov et al. (2017) presented a related approach based on probabilistic movement primitives, which jointly solves the segmentation and learning step for an unknown number of primitives in an expectation-maximization framework. Yet, the model operates purely on the trajectory level and cannot provide insights in to the latent intention of the demonstrator. Another variant of the approach by Niekum et al. (2012), which explicitly addresses this problem, was proposed by Surana and Srivastava (2014). In their paper, the authors propose to replace the HMM emission model with an MDP model, in order to infer a policy from the segmented trajectories rather than to recognize changes in the dynamics. The model was later extended by Ranchod et al. (2015), who augmented the HMM representation with a beta process model to facilitate skill sharing across trajectories. While the resulting formulation is very flexible, a major drawback of the model is that inference is computationally expensive since it involves multiple IRL iterations per Gibbs step.

In contrast to the HMM-based solutions, which by their sequential nature focus on the *temporal* relationship of the subtasks, the approach presented in this paper establishes a correlation structure between the demonstrations without committing to a temporal factorization of the subgoals, using a non-exchangeable distribution over subgoal assignments. This results in a compact model representation (e.g., it avoids the need of estimating subgoal transition probabilities) and brings the flexibility to capture both, the temporal and the spatial dependencies between the subtasks.

## 1.2 Paper Outline

The organization of the remaining sections is as follows: in Section 2, we summarize the BNIRL model, which forms the basis for our work. Section 3 then introduces our new intentional subgoal framework, which addresses the shortcomings of BNIRL discussed in Section 2. In Section 4, we derive a sampling-based inference scheme for our model and explain how the new framework can be used for subgoal extraction and action prediction.

Experimental results on both synthetic and real-world data are presented in Section 5, before we finally conclude our work in Section 6.

## 2. Bayesian Nonparametric Inverse Reinforcement Learning

The purpose of this section is to recapitulate the principle of Bayesian nonparametric inverse reinforcement learning. After briefly discussing all building blocks of the model, we focus on the limitations of the framework, which motivates the need for an extended model formulation and finally leads to a new inference approach, presented afterwards in Section 3.

### 2.1 Revisiting the BNIRL Framework

Following the common IRL paradigm (Ng and Russell, 2000; Zhifei and Joo, 2012), the goal of BNIRL is to infer the intentions of an agent from demonstration data. Starting from the standard MDP model, the problem is formalized on a finite state space  $\mathcal{S}$  assuming a time-invariant state transition model  $T : \mathcal{S} \times \mathcal{S} \times \mathcal{A} \rightarrow [0, 1]$ , where  $\mathcal{A}$  is a finite set of actions available to the agent at each state. For notational convenience, we represent the states in  $\mathcal{S}$  by the integer values  $\{1, \dots, |\mathcal{S}|\}$ , where  $|\mathcal{S}|$  denotes the cardinality of the state space.

In BNIRL, it is assumed that we observe a number of expert demonstrations, provided in the form of state-action pairs,  $\mathcal{D} := \{(s_d, a_d)\}_{d=1}^D$ , where each pair  $(s_d, a_d) \in \mathcal{S} \times \mathcal{A}$  consists of a state  $s_d$  visited by the agent and the corresponding action  $a_d$  taken. Herein,  $D$  denotes the size of the demonstration set. Throughout the rest of this paper, we will use the shorthand notations  $\mathbf{s} := \{s_d\}_{d=1}^D$  and  $\mathbf{a} := \{a_d\}_{d=1}^D$  to access the collection of expert states and actions individually. Note that the BNIRL model makes no assumptions on the temporal ordering of the demonstrations, i.e., each state-action pair is considered to arise from a specific but arbitrary time instant of the agent’s decision-making process. We will come back to this point later in Section 2.2 and Section 3.3.

In contrast to the classical MDP formalism and most other IRL frameworks, BNIRL does *not* presuppose that the observed expert behavior necessarily originates from a single underlying reward function. Instead, it introduces the concept of *subgoals* (and corresponding *subgoal assignments*) with the underlying assumption that, at each decision instant, the expert selects a particular subgoal to plan the next action. Each subgoal is herein represented by a certain reward function defined on the system state space; in the simplest case, it corresponds to a single reward mass placed at a particular goal state in  $\mathcal{S}$ , which we identify with a reward function  $R_g : \mathcal{S} \rightarrow \{0, C\}$  of the form

$$R_g(s) := \begin{cases} C & \text{if } g = s, \\ 0 & \text{otherwise,} \end{cases} \quad (1)$$

where  $g \in \{1, \dots, |\mathcal{S}|\}$  indicates the respective subgoal location and  $C \in (0, \infty)$  is some positive constant (compare Şimşek et al., 2005; Stolle and Precup, 2002; Tamassia et al., 2015).

Although in principle it is legitimate to associate each subgoal with an arbitrary reward structure in order to encode more complex forms of goal-oriented behavior (see, for example, Ranchod et al., 2015), the restriction to the reward function class in Equation (1) is sufficient in that the same behavioral complexity can be synthesized through the combination of several subgoals. This is made possible by the nonparametric nature of the

BNIRL model, i.e., because the number of subgoals is assumed to be unbounded. The use of the simple reward model has the advantage, however, that posterior inference about the subgoals targeted by the expert becomes computationally tractable, as will be explained in Section 4.5. In the following, we therefore assume the reward model in Equation (1) and summarize the infinite collection of subgoals in the multiset  $\mathcal{G} := \{g_k\}_{k=1}^\infty \in \times_{k=1}^\infty \mathcal{S}$ , where we adopt the assumption that  $p(\mathcal{G} | \mathbf{s}) = \prod_{k=1}^\infty p_g(g_k | \mathbf{s})$ .<sup>1</sup>

The subgoal assignment in BNIRL is implemented using a set of indicator variables  $\tilde{\mathbf{z}} := \{\tilde{z}_d \in \mathbb{N}\}_{d=1}^D$  that annotate each demonstration pair  $(s_d, a_d)$  with its unique subgoal index. The prior distribution  $p(\tilde{\mathbf{z}})$  is herein modeled by a Chinese restaurant process (CRP, Aldous, 1985), which assigns the event that indicator  $\tilde{z}_d$  points to the  $j$ th subgoal the prior probability

$$p(\tilde{z}_d = j | \tilde{\mathbf{z}}_{\setminus d}) \propto \begin{cases} n_j & \text{if } j \in \{1, \dots, K\}, \\ \alpha & \text{if } j = K + 1, \end{cases}$$

where  $\tilde{\mathbf{z}}_{\setminus d} := \{\tilde{z}_d\} \setminus \tilde{z}_d$  is a shorthand notation for the collection of all indicator variables without  $\tilde{z}_d$ . Further,  $n_j$  denotes the number of assignments to the  $j$ th subgoal in  $\tilde{\mathbf{z}}_{\setminus d}$ ,  $K$  represents the number of distinct entries in  $\tilde{\mathbf{z}}_{\setminus d}$ , and  $\alpha \in [0, \infty)$  is a parameter controlling the diversity of the assignments.

Having targeted a particular subgoal  $g_{\tilde{z}_d}$  while being at some state  $s_d$ , the expert is assumed to choose the next action  $a_d$  according to a softmax decision rule,  $\pi : \mathcal{A} \times \mathcal{S} \times \mathcal{S} \rightarrow [0, 1]$ , which weighs the expected returns of all actions against one another,

$$\pi(a_d | s_d, g_{\tilde{z}_d}) := \frac{\exp\{\beta Q^*(s_d, a_d | g_{\tilde{z}_d})\}}{\sum_{a \in \mathcal{A}} \exp\{\beta Q^*(s_d, a | g_{\tilde{z}_d})\}}. \quad (2)$$

Herein,  $Q^*(s, a | g)$  denotes the state-action value (or *Q-value*, Sutton and Barto, 1998) of action  $a$  at state  $s$  under an optimal policy for the subgoal reward function  $R_g$ ,

$$Q^*(s, a | g) := \max_{\pi} \mathbb{E} \left[ \sum_{n=0}^{\infty} \gamma^n R_g(s_{t=n}) \mid s_{t=0} = s, a_{t=0} = a, \pi \right], \quad (3)$$

where the expectation is with respect to the stochastic state sequence of the expert generated under policy  $\pi$  with initial action  $a$  executed at the starting state  $s$ . The explicit notation  $s_{t=n}$  and  $a_{t=n}$  is used to disambiguate the temporal index of the decision-making process from the demonstration index of the state-action pairs  $\{(s_d, a_d)\}$ .

The softmax policy  $\pi$  models the expert’s ability to maximize the future expected return in view of the targeted subgoal, while the coefficient  $\beta \in [0, \infty)$  is used to express the expert’s level of confidence in the optimal action. Combined with the subgoal prior distribution  $p(g_k | \mathbf{s})$  and the partitioning model  $p(\tilde{\mathbf{z}})$ , we obtain the joint distribution of all demonstrated actions  $\mathbf{a}$ , subgoals  $\mathcal{G}$ , and subgoal assignments  $\tilde{\mathbf{z}}$  as

$$p(\mathbf{a}, \tilde{\mathbf{z}}, \mathcal{G} | \mathbf{s}) = p(\tilde{\mathbf{z}}) \prod_{k=1}^{\infty} p_g(g_k | \mathbf{s}) \prod_{d=1}^D \pi(a_d | s_d, g_{\tilde{z}_d}). \quad (4)$$

---

1. Notice that the subgoal prior distribution in the original BNIRL formulation does not take the state variable  $\mathbf{s}$  as an argument. Nonetheless, the authors of BNIRL suggest to restrict the support of the prior to the set of visited states, which indeed implies a conditioning on  $\mathbf{s}$ .

The structure of this distribution is visualized in form of a graphical model in Figure 5a. It is worth emphasizing that  $\pi$ —although it is referred to as the likelihood model for the state-action *pairs* in the original BNIRL paper—is really just a model for the actions *conditional on the states*. In contrast to what is stated in the original paper, the distribution in Equation (4) therefore takes the form of a *conditional* distribution (i.e., conditioned on  $\mathbf{s}$ ), which does not provide any generative description for the state variables.

Posterior inference in the BNIRL model refers to the (approximate) computation of the conditional distribution  $p(\tilde{\mathbf{z}}, \mathcal{G} \mid \mathcal{D})$ , which allows to identify potential subgoal locations and the corresponding subgoal assignments based on the available demonstration data. For further details, the reader is referred to the original paper (Michini and How, 2012).

## 2.2 Limitations of BNIRL

Subgoal-based inference is a well-motivated approach to IRL and the BNIRL framework has shown promising results in a variety of real-world scenarios. Yet, the original model formulation by Michini and How (2012) comes with a number of significant conceptual limitations, which we explain in detail in the following paragraphs.

### 2.2.1 LIMITATION 1: SUBGOAL EXCHANGEABILITY AND POSTERIOR PREDICTIVE POLICY

The central limitation of BNIRL is that the framework is restricted to pure subgoal extraction and does *not* inherently provide a suitable mechanism to forecast the expert behavior based on the inferred subgoals. The reason lies in the particular design of the framework which, at its heart, treats the subgoal assignments  $\tilde{\mathbf{z}}$  as *exchangeable random variables* (Aldous, 1985). By implication, the induced partitioning model  $p(\tilde{\mathbf{z}})$  is agnostic about the covariate information in the data set and the resulting behavioral model is unable to reasonably propagate the expert knowledge to new situations.

To illustrate the problem, let us investigate the predictive action distribution that arises from the original BNIRL formulation. For simplicity and without loss of generality, we may assume that the model has perfectly inferred all subgoals  $\mathcal{G}$  and corresponding subgoal assignments  $\tilde{\mathbf{z}}$  from the demonstration set. Denoting by  $a^* \in \mathcal{A}$  the predicted action at some new state  $s^* \in \mathcal{S}$ , the BNIRL model yields

$$\begin{aligned} p(a^* \mid s^*, \mathcal{D}, \tilde{\mathbf{z}}, \mathcal{G}) &= \sum_{\tilde{z}^* \in \mathbb{N}} p(a^*, \tilde{z}^* \mid s^*, \mathcal{D}, \tilde{\mathbf{z}}, \mathcal{G}) \\ &= \sum_{\tilde{z}^* \in \mathbb{N}} p(a^* \mid \tilde{z}^*, s^*, \mathcal{D}, \tilde{\mathbf{z}}, \mathcal{G}) p(\tilde{z}^* \mid s^*, \mathcal{D}, \tilde{\mathbf{z}}, \mathcal{G}) \\ &\stackrel{(\star)}{=} \sum_{\tilde{z}^* \in \mathbb{N}} p(a^* \mid \tilde{z}^*, s^*, g_{\tilde{z}^*}) p(\tilde{z}^* \mid \tilde{\mathbf{z}}), \end{aligned} \quad (5)$$

where  $\tilde{z}^* \in \mathbb{N}$  is the latent subgoal indicator belonging to  $s^*$ . Herein,  $p(a^* \mid \tilde{z}^*, s^*, g_{\tilde{z}^*})$  can either represent the softmax decision rule  $\pi(a^* \mid s^*, g_{\tilde{z}^*})$  from Equation (2) or the optimal (deterministic) policy for subgoal  $g_{\tilde{z}^*}$ , depending on whether we aspire to describe the *noisy expert behavior* at  $s^*$  or want to determine the *optimal action* according to the inferred reward model. Note that the last equality in Equation (5), indicated by  $(\star)$ , follows from the

conditional independence properties implied by Equation (4), which can be easily verified using d-separation (Koller and Friedman, 2009) on the graphical model in Figure 5a.

As Equation (5) reveals, the predictive model is characterized by the posterior distribution  $p(\tilde{z}^* | s^*, \mathcal{D}, \tilde{\mathbf{z}}, \mathcal{G})$  of the latent subgoal assignment  $\tilde{z}^*$  of state  $s^*$ ; the intuition being that, in order to generalize the expert’s plan to a new situation, we need to take into account the gathered information about what would be a likely subgoal targeted by the expert at  $s^*$ . However, in BNIRL, the distribution  $p(\tilde{z}^* | s^*, \mathcal{D}, \tilde{\mathbf{z}}, \mathcal{G})$  is modeled *without consideration of the query state  $s^*$ , or any other observed variable*. By conditional independence (Equation 4), the distribution effectively reduces (★) to the CRP prior  $p(\tilde{z}^* | \tilde{\mathbf{z}})$ , which due to its intrinsic exchangeability property only considers the frequency of the readily inferred assignments  $\tilde{\mathbf{z}}$ . Clearly, a subgoal selection strategy based solely on relative frequencies is of little use when it comes to predicting the expert behavior at a new state: the resulting subgoal assignment mechanism will inevitably ignore the structural information of the demonstration set and consistently produce the same subgoal assignment probabilities at all states, irrespective of the agent’s actual situation. By contrast, a reasonable assignment mechanism should inherently take into account the context of the agent’s current state  $s^*$  when deciding about the next action.

While the authors of BNIRL discuss the action selection problem in their paper and propose a subgoal assignment strategy for new states based on action marginalization, their approach does not provide a satisfactory solution to the problem because the alleged conditioning on the query state (see Equation 19 in the original paper by Michini and How, 2012) has no effect on the involved subgoal indicator variable, as shown by Equation (5). The only way to remedy the problem without modifying the model is via an external post-processing scheme like the waypoint method, which we discuss in the next section.

### 2.2.2 LIMITATION 2: SPATIAL AND TEMPORAL CONTEXT

The waypoint method, described at full length in a follow-up paper by Michini et al. (2015), is a post-processing routine that converts the subgoals identified through BNIRL into a valid option model (Sutton et al., 1999), based on the spatio-temporal information contained in the demonstration set. For this purpose, the required initiation and termination sets of the option-policies are constructed via the state proximities to the identified subgoals and their temporal ordering as prescribed by the expert.

When combined with BNIRL, the method allows to synthesize a behavioral model that mimics the observed expert behavior. However, this strategy comes with a number of significant drawbacks: (i) using the waypoint method, the spatio-temporal context is explored only in a post-hoc fashion and is largely ignored during the actual inference procedure (the state information enters via the likelihood model  $\pi$  but is not considered in the partitioning model  $p(\tilde{\mathbf{z}})$ , as explained in Limitation 1). This lack of context-awareness makes the inference mechanism overly prone to demonstration noise (see Figure 1 and results in Section 5). (ii) Measuring proximities to subgoals in order to determine their visitation order requires some form of distance metric defined on the state space. If the system states correspond to physical locations, constructing such a metric is usually straightforward. However, in the general case, where states may encode arbitrary abstract information (see Section 5.2), it can become difficult to design that metric by hand. Unfortunately, the BNIRL frame-

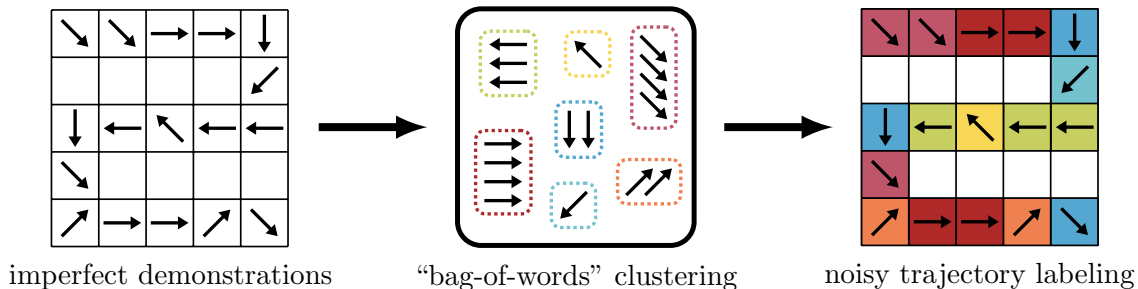


Figure 1: A schematic to illustrate the implications of the exchangeability assumption in BNIRL. Similar to a “bag-of-words” model (Blei et al., 2003; Yang et al., 2007), the BNIRL partition assignment mechanism ignores the spatio-temporal context of the data, which makes it difficult to discriminate demonstration noise from a real change of the agent’s intentions. Note that the schematic illustrates the partitioning process in a simplified way as it only shows the effect of the prior  $p(\bar{\mathbf{z}})$  but neglects the impact of the likelihood model  $\pi$ . While the latter *does* indeed consider the state context of the actions, it cannot account for any spatial or temporal patterns in the data set as it processes all state-action pairs separately.

work does not provide any solution to this problem. (iii) The waypoint method cannot be applied to multiple unaligned trajectories (e.g., obtained from different experts) or in cases where the data set does not contain any temporal information. This situation occurs, for instance, when the data is not provided in form of trajectories but given as individual state-action pairs recorded at arbitrary time points. (iv) Assigning a particular order to the inferred subgoals is meaningful only if the expert eventually reaches those subgoals during the demonstration phase (or if, at least, the subgoals lie “close” to the visited states in terms of the aforementioned distance metric). Finding subgoals with such properties can be guaranteed by constraining the support of the subgoal prior distribution  $p_g$  to states that are near to the expert states (see footnote on page 6) but this reduces the flexibility of the model and potentially disables compact encodings of the task (Figure 2).

### 2.2.3 LIMITATION 3: INCONSISTENCY UNDER TIME-INVARIANCE

Reasoning about the intentions of an agent, there are two basic types of behavior one may encounter: (i) either the agent follows a static strategy to optimize a fixed objective (as assumed in the standard MDP formalism, Sutton and Barto, 1998) or (ii) the intentions of the agent change with time. The latter is clearly the more general case but also poses a more difficult inference problem in that it requires us both, to identify the intentions of the agent and to understand their temporal relationship. The static scenario, in contrast, implies that there exists an optimal policy for the task in form of a simple state-to-action mapping (Puterman, 1994),  $\pi : \mathcal{S} \rightarrow \mathcal{A}$ , which from the very beginning imprints a specific structure on the inference problem.

The BNIRL model generally falls into the second category since it freely allocates its subgoals per *decision instant* and not per state, allowing a flexible change of the agent’s

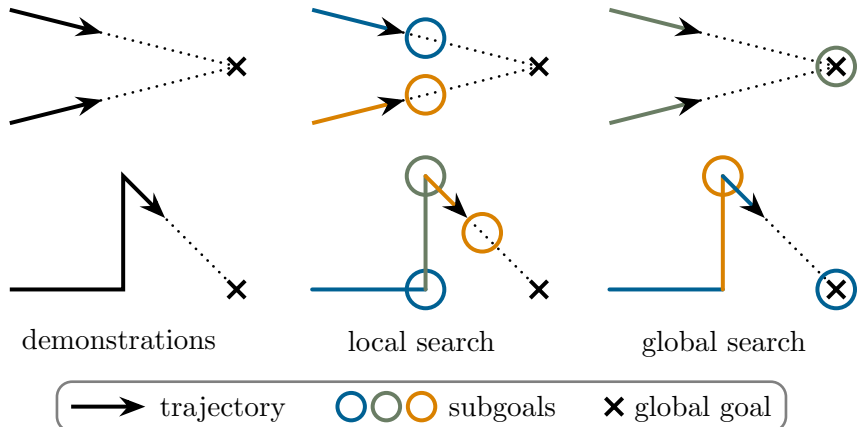


Figure 2: Difference between local (constrained) and global (unconstrained) subgoal search. **Top:** two trajectories approaching the same goal. **Bottom:** an agent is heading towards a global goal, gets temporarily distracted, and then follows up on its original plan. **Left:** observed trajectories. **Center:** example partitioning under the assumption that the expert reached all subgoals during the demonstration. **Right:** example partitioning without restriction on the subgoal locations, yielding a more compact encoding of the task.

objective. Yet, it is important to understand that the model does not actually distinguish between the two described scenarios. As explained in Limitation 2, the temporal aspect of the data is not explicitly modeled by the BNIRL framework, even though the waypoint method subsequently tries to capture the overall chronological order of events. As a consequence, the model is not tailored to either of the two settings: on the one hand, it ignores the valuable temporal context which is needed in the time-varying case to reliably discriminate demonstration noise from a real change of the agent’s intention. On the other hand, the model is agnostic about the predefined time-invariant nature of the optimal policy in the static scenario. This lack of structure not only makes the inference problem harder than necessary in both cases; it also allows the model to learn inconsistent data representations in the static case since the same state can be potentially assigned to more than one subgoal, violating the above-mentioned state-to-action rule (Figure 3).

#### 2.2.4 LIMITATION 4: ACTION LIKELIHOOD MODEL

Apart from the discussed limitations of the BNIRL partitioning model, it turns out there are two major issues concerning the softmax likelihood model (Equation 2). On the subsequent pages, we will demonstrate that the specific form of this model encodes a number of properties that contradict our intuitive understanding of the subgoal inference problem. While these properties are less critical for the actual prediction of the expert behavior, they drastically affect the *localization* of subgoals. Since the cause of these effects is somewhat hidden in the equation, we defer their detailed explanation to Section 3.1.

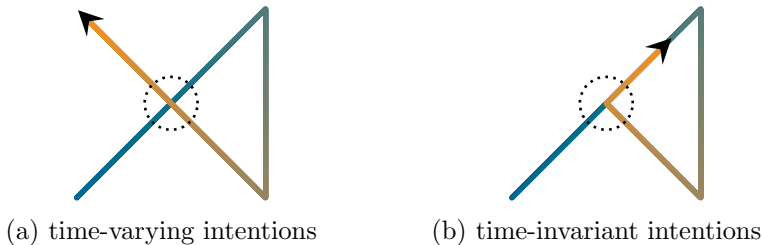


Figure 3: Schematic comparison of the two basic behavior types. (a) Time-varying intentions may cause the agent to perform a different action when revisiting a state. (b) By contrast, time-invariant intentions imply a simple state-to-action policy: the agent has no incentive to perform a different action at an already visited state since, by assumption, the underlying goals have remained unchained. Diverging actions, as they occur at the trajectory crossing point in (a), can therefore only be explained as a result of suboptimal behavior.

### 2.2.5 LIMITATION 5: STATE-ACTION DEMONSTRATIONS

A minor problem of the original BNIRL problem formulation is that the algorithm expects the demonstration data to be provided in the form of state-action pairs, which requires full access to the expert’s action record. This assumption is restrictive from a practical point of view as it confines the application of the framework to settings with laboratory-like conditions that allow for a complete monitoring of the expert. For this reason, it is important to note that an estimate of the actions can be recovered through BNIRL with the help of an additional sampling stage (omitted in the original paper), provided that we know the successor state reached by expert after each decision step. For the marginalized sampling scheme described in this paper, we present the corresponding action sampling stage in Section 4.4.

## 3. Nonparametric Spatio-Temporal Subgoal Modeling

In this section, we introduce a redesigned inference framework, which we by analogy to BNIRL refer to as *distance-dependent Bayesian nonparametric IRL* (ddBNIRL). We derive the model by making a series of modifications to the original BNIRL framework that address the previously described shortcomings on the conceptual level. Rethinking each part of the BNIRL model, we begin with a discussion of the commonly used softmax action selection strategy (Equation 2) in the context of subgoal inference, which finally leads to a redesign of the action likelihood model (Limitation 4). Next, we focus on the subgoal allocation mechanism itself and introduce two closely related model formulations, each targeting one of the basic behavior types described in Figure 3, thereby addressing Limitations 1, 2 and 3. For the time-invariant case, we begin with an intermediate model that introduces a subtle yet important structural modification to the BNIRL framework. In a second step, we generalize that new model to account for the structure of the control problem itself, which finally allows us to extrapolate the expert behavior to unseen situations. In this context, we present a new state space metric that arises naturally in the context of subgoal inference

(see details of Limitation 2). Lastly, we tackle the time-varying case and present a variant of the model that explicitly considers the temporal aspect of the problem. A solution to Limitation 5 is discussed later in Section 4.

In contrast to BNIRL, both presented models can be used likewise for *subgoal extraction* and *action prediction*. Moreover, sticking with the Bayesian methodology, the presented approach provides complete posterior information at all levels.

### 3.1 The Action Likelihood Model

Like many other approaches found in the IRL literature, BNIRL exploits a softmax weighting (Equation 2) to transform the Q-values of an optimal policy into a valid action likelihood model. The softmax action rule has its origin in reinforcement learning where it is known as the Boltzmann exploration strategy, (Cesa-Bianchi et al., 2017; Sutton and Barto, 1998), which is commonly applied to cope with the *exploration-exploitation dilemma* (Ghavamzadeh et al., 2015). In recent years, however, it has also become the de facto standard for modeling the (imperfect) decision-making process of an agent (see, for example, Dimitrakakis and Rothkopf, 2011; Ramachandran and Amir, 2007; Rothkopf and Dimitrakakis, 2011; Choi and Kim, 2012; Neu and Szepesvári, 2007; Babes-Vroman et al., 2011).

In the following paragraphs, we focus on the implications of this model on the subgoal extraction problem and show that it contradicts our understanding of what characteristics a reasonable subgoal model should have. In particular, we argue that the subgoal posterior distribution arising from the BNIRL softmax model is of limited use for inferring the latent intention of the agent, due to subgoal artifacts caused by the system dynamics that do not reflect the evidence contained in demonstration set. Based on these insights, we propose an alternative transformation scheme that is more consistent with the subgoal principle.

#### 3.1.1 SCALE OF THE REWARD FUNCTION

The first implication of the softmax likelihood model concerns the choice of the uncertainty coefficient  $\beta$ . To explain the problem, we consider the thought experiment of an agent located at some state  $s$  targeting a particular subgoal  $g$ . The likelihood  $\pi(a | s, g)$  in Equation (2) quantifies the probability that the agent decides for a specific action  $a$ , based on the corresponding Q-values  $Q(\cdot, s | g)$ . Since these values are linear in the underlying reward function  $R_g$  (Equation 3), the softmax likelihood model implies that the expert’s ability to maximize the long-term reward—as reflected by the distribution of the probability mass in  $\pi(\cdot | s, g)$ —rises with the magnitude  $C$  of the assumed subgoal reward. In other words, assuming a higher goal reward virtually increases our level of confidence in the expert, even though the difficulty of the underlying task and the optimal policy remain unchanged. Nonetheless, the BNIRL model requires us to readjust the uncertainty coefficient  $\beta$  in order to keep both models consistent. Because the BNIRL model provides no reference level for the expert’s uncertainty across different scenarios, the choice of  $\beta$  becomes non-trivial. Yet, the parameter has a significant impact on the granularity of the learned subgoal model as it trades off purposeful goal-oriented behavior against random decisions.

Note that the described effect is not specific to the subgoal reward model in Equation (1) but arises in any MDP setting with arbitrary reward function, for example, when we provide an additional constant reward at all states. Clearly, such a reward function provides no

additional information about the underlying task and should hence not affect the agent’s belief about the optimal choice of actions (c.f. discussion on constant reward functions and transformations of rewards, Ng and Russell, 2000; Ng et al., 1999). Based on these two observations, our intuition tells us that we seek for a model of rationality that is *invariant to affine transformations of the reward signal*, meaning that any two reward functions  $R$  and  $\bar{R} := xR + y$ ,  $x, y \in \mathbb{R}$ , should give rise to the same behavioral model. As we shall see in Section 3.1.3, this can be achieved by modeling the behavior of an agent based on the *relative advantages* of actions rather than on their absolute returns.

### 3.1.2 IMPACT OF THE TRANSITION DYNAMICS

The second implication of the softmax likelihood model is less immediate and inherently tied to the dynamics of the system. To explain the problem, we consider a generic scenario where we have a precise idea about the potential goals of the expert. For our example, we adopt the grid world model described in Section 5.1 and consider a simple upward-directed trajectory of state-action pairs, which we aspire to explain using a single (sub)goal. The complete setting is depicted in Figure 4. Intuitively, the shown demonstration set should give rise to goals that are located in the upper region of the state space and concentrated around the vertical center line. Moreover, as we move away from the center line, we expect to see a smooth decrease in the subgoal likelihood while the rate of the decay should reflect our assumed level of confidence in the expert. As it turns out, the induced BNIRL subgoal posterior distribution, shown in the top row for different values of  $\beta$ , contradicts this intuition. In particular, we observe that the likelihood model yields unreasonably high posterior values at the upper border states and corners of the state space which, according to our intuitive understanding of subgoals, cannot be justified by the given demonstration set.

To pin down the cause of this effect, we recall from Equation (2) that the likelihood of an action grows with the Q-value of that action. Hence, we need to ask what causes the Q-values of the demonstrated actions to be large if we assume the subgoal to be located at one of the corner states. Using Bellman’s principle, we can express the Q-values for any given policy  $\pi$  as

$$\begin{aligned} Q^\pi(s, a | g) &= R_g(s) + \gamma \mathbb{E}_T[V^\pi(s' | g) | s, a] \\ &= R_g(s) + \gamma \mathbb{E}_T[\mathbb{E}_{\rho^\pi}[R_g(s'') | s'] | s, a] \\ &= R_g(s) + \gamma \mathbb{E}_T[C\rho^\pi(g | s') | s, a], \end{aligned} \tag{6}$$

where  $V^\pi(s | g) = \max_{a \in \mathcal{A}} Q^\pi(s, a | g)$ , and  $C$  is the subgoal reward from Equation (1). Further,  $\rho^\pi(s' | s) := \sum_{t=0}^{\infty} \gamma^t p_t(s' | s, \pi)$  denotes the (improper) discounted state visitation distribution generated by executing policy  $\pi$  from the considered initial state  $s$ , where  $p_t(s' | s, \pi)$  refers to the probability of reaching state  $s'$  from state  $s$  under policy  $\pi$  after exactly  $t$  steps, which is defined implicitly via the transition model  $T$ .

The outer expectation in Equation (6) accounts for the stochastic transition to the successor state  $s'$ , while the inner expectation evaluates the expected cumulative reward over all states  $s''$  that are reachable from  $s'$ . It is important to note that—by the construction of the Q-function—only the first move of the agent to state  $s'$  depends on the choice of action  $a$  whereas all remaining moves (i.e., the inner part of the last expectation) are purely driven by the system dynamics/the subgoal policy. Focusing on that inner part, we conclude that,

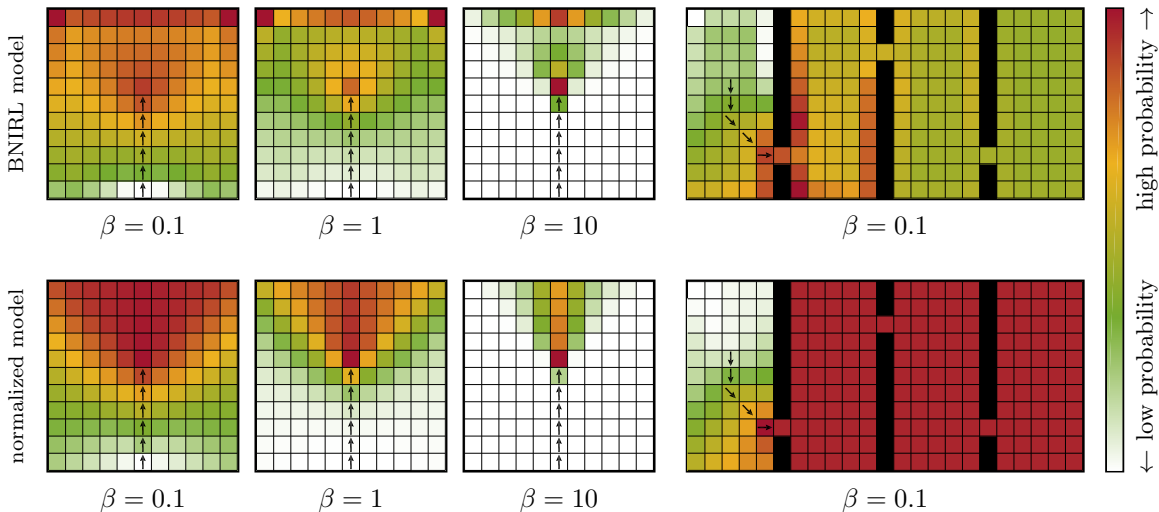


Figure 4: Comparison of the subgoal posterior distributions induced by the original BNIRL likelihood model (top row) and by the proposed normalized model (bottom row), based on the grid world dynamics described in Section 5.1 and a uniform subgoal prior distribution. The range of the shown color scheme is to be understood per subfigure. Black squares indicate wall states. The BNIRL likelihood model yields unreasonably high subgoal posterior mass at the border states and corners of the state space, due to locally increased state visitation probabilities arising from wall reflections, as well as at the trajectory ending, caused by the implicit proximity property of the model. Both effects are mitigated by the proposed normalized likelihood because it models the action selection process of the expert using the relative advantages of the available actions instead of their absolute returns.

irrespective of the chosen action, the Q-values will be large whenever the subgoal induces a high state visitation frequency  $\rho^\pi$  at its own location  $g$ . The latter is fulfilled if (i) the chance of reaching the goal in a small number of steps is high so that the effect of the discounting is small and/or when (ii) the subgoal-induced transition dynamics

$$p(s' | s, g) := \sum_{a \in \mathcal{A}} T(s' | s, a) \pi(a | s, g)$$

give rise to a high goal visitation frequency itself. Note that the first condition implies that the model generally prefers subgoals which are close to the demonstration set—a property which cannot be justified in all cases. For example, the recording of the demonstrations could have simply ended before the expert was able to reach the goal (recall Figure 3). However, if desired, this proximity property should be more naturally attributed to the subgoal prior model  $p_g(g | \mathbf{s})$ .

In our example in Figure 4, we can observe the effects of both described conditions clearly. In particular, for an upward-directed policy as implied by the shown demonstration set, the state visitation distribution  $\rho^\pi$  exhibits increased values at exactly the aforementioned border and corner states (due to the reflections occurring to the agent when hitting

the state space boundary) as well as close to the trajectory ending (caused by the proximity condition).

### 3.1.3 THE NORMALIZED LIKELIHOOD MODEL

To address these problems, we propose to modify the likelihood model using a rescaling of the involved Q-values. Let  $Q^\wedge(s|g)$  and  $Q^\vee(s|g)$  denote the maximum and minimum Q-values at state  $s$  for subgoal  $g$ , that is,  $Q^\wedge(s|g) := \max_{a \in \mathcal{A}} Q^*(s, a|g)$  and  $Q^\vee(s|g) := \min_{a \in \mathcal{A}} Q^*(s, a|g)$ . We then define the normalized state-action value function  $Q^\bullet : \mathcal{S} \times \mathcal{A} \times \mathcal{S} \rightarrow [0, 1]$  as

$$Q^\bullet(s, a|g) := \begin{cases} \frac{Q^*(s, a|g) - Q^\vee(s|g)}{Q^\wedge(s|g) - Q^\vee(s|g)} & \text{if } Q^\wedge(s|g) \neq Q^\vee(s|g), \\ \epsilon & \text{otherwise,} \end{cases} \quad (7)$$

where  $\epsilon \in (0, 1]$  is an arbitrary constant that is canceled out in Equation (8). In contrast to the Bellman state-action value  $Q^*$ , which describes the (expected) return of an action, the normalized function  $Q^\bullet$  assesses the return of that action in relation to the returns of all other actions. This concept is similar to that of the advantage function (Baird, 1993) with the important difference that the values returned by  $Q^\bullet$  are normalized to the range  $[0, 1]$  and thus serve as an indicator for the *relative* quality of an action. As such, they can be interpreted as *relative advantages* (i.e., relative to the maximum possible advantage among all actions). The normalized action likelihood model is then constructed analogously to the BNIRL likelihood model,

$$\pi^\bullet(a_d | s_d, g\bar{z}_d) \propto \exp \{ \beta Q^\bullet(s_d, a_d | g\bar{z}_d) \}. \quad (8)$$

The key property of this model is that it is invariant to affine transformations of the reward function, as summarized by the following proposition.

**Proposition 1 (Affine Invariance)** *Consider an MDP with reward function  $R : \mathcal{S} \rightarrow \mathbb{R}$  and let  $Q^*(s, a|R)$  denote the corresponding optimal state-action value function. It holds that  $Q^\bullet(s, a|R) = Q^\bullet(s, a|xR + y) \forall x, y \in \mathbb{R}, s \in \mathcal{S}, a \in \mathcal{A}$ . Hence, the normalized action likelihood model in Equation (8) is invariant to affine transformations of  $R$ .*

**Proof** Due to the linear dependence of  $Q^*$  on the reward function  $R$  (Equation 3) it holds that  $Q^*(s, a|xR + y) = xQ^*(s, a|R) + \frac{y}{1-\gamma}$ . Using this relationship in Equation (7), it follows immediately that  $Q^\bullet(s, a|R) = Q^\bullet(s, a|xR + y)$ .  $\blacksquare$

Using the proposed likelihood model offers several advantages. First of all, the normalization enables a more generic choice of the uncertainty coefficient  $\beta$  (Section 3.1.1). This is because the returned  $Q^\bullet$ -values lie in the fixed range  $[0, 1]$ , where 0 always indicates the lowest and 1 the highest confidence. For example, setting  $\beta = \log(\beta')$  for some  $\beta' \in (0, \infty)$  always reflects the assumption that the expert chooses the optimal action with a probability that is  $\beta'$  times higher than the probability of choosing the least favorable action, irrespective of the underlying system model.

Moreover, as the bottom row in Figure 4 reveals, the induced posterior distribution is notably closer to our expectation. The reason for this is twofold: first, a likelihood computation based on relative advantages mitigates the influence of the transition dynamics discussed in Section 3.1.2. This is because the described cumulation effect of the state visitation distribution (Equation 6) is present in the returns of all actions and thus reduced through the normalization. Second, since the normalization diminishes the effect of the discounting, the posterior subgoal mass is less concentrated around the trajectory ending and shows a significant probability along the extrapolated path of the agent. This property allows us to identify far located states as potential subgoals which adds more flexibility to the inferred subgoal constellation (Figure 2). As an example, consider the rightmost subfigures in Figure 4. We observe that the normalized model assigns high posterior mass to all states in the right three corridors since all subgoals located in these areas explain the demonstration set equally well. Here, the difference between the two models is even more pronounced because the transition dynamics have a strong impact on the agent behavior due to the added wall states. For further details, we refer to Section 5.1, where we provide additional insights into the subgoal inference mechanism.

### 3.2 Modeling Time-Invariant Intentions

With our redesigned likelihood model, we now focus on the partitioning structure of the model. Herein, we first consider the case where the intentions of the agent are constant with respect to time. As explained in Limitation 3, this setting is consistent with the standard MDP formalism, meaning that the optimal policy for the considered task can be described in the form of a state-to-action mapping.

As a first step, we thus establish a link between the model partitioning structure and the underlying system state space by replacing the demonstration-based indicators  $\tilde{\mathbf{z}} = \{\tilde{z}_d \in \mathbb{N}\}_{d=1}^D$  with a new set of variables  $\mathbf{z} := \{z_i \in \mathbb{N}\}_{i=1}^{|\mathcal{S}|}$ . Unlike  $\tilde{\mathbf{z}}$ , these variables do not operate directly on the data set but are instead tied to the elements in  $\mathcal{S}$ . Although they formally represent a new type of variable, we can still imagine that they are generated through a CRP. This yields an intermediate model of the form

$$p(\mathbf{a}, \mathbf{z}, \mathcal{G} | \mathbf{s}) = p(\mathbf{z}) \prod_{k=1}^{\infty} p_g(g_k | \mathbf{s}) \prod_{d=1}^D \pi^\bullet(a_d | s_d, g_{\mathbf{z}_{s_d}}),$$

whose structure is illustrated in Figure 5b. Notice the way in which the subgoals are indexed in this model compared to Equation (4).

The intermediate model makes it possible to reason about the policy (or, more suggestively, the underlying state-to-action rule approximated by the expert) at visited parts of the state space. Yet, the model is unable to extrapolate the gathered information to unvisited states, for the reasons explained in Section 2.2. This problem can be solved by replacing the exchangeable prior distribution over subgoal assignments induced by the CRP with a non-exchangeable one, in order to account explicitly for the covariate state information of the demonstrations. Based on our insights from Bayesian policy recognition (BPR, ŠošiĆ et al., 2018b), we use the distance-dependent Chinese restaurant process (ddCRP, Blei and Frazier, 2011) for this purpose, which allows a very intuitive handling of the covariate information, as will be explained below. Note that there exist a variety of other choices

with different properties, but a further discussion lies outside the scope of this work. For more details, we point to the excellent survey paper by [Foti and Williamson \(2015\)](#).

In contrast to the CRP, which assigns states to partitions, the ddCRP assigns states to other states, based on their pairwise distances. These “to-state” assignments are described by a set of indicators  $\mathbf{c} := \{c_i \in \mathcal{S}\}_{i=1}^{|\mathcal{S}|}$  with prior distribution  $p(\mathbf{c}) = \prod_{i=1}^{|\mathcal{S}|} p(c_i)$ ,

$$p(c_i = j) = \begin{cases} \nu & \text{if } i = j, \\ f(\Delta_{i,j}) & \text{otherwise,} \end{cases}$$

for  $i, j \in \mathcal{S}$ . Herein,  $\nu \in [0, \infty)$  is called the self-link parameter of the process,  $\Delta_{i,j}$  denotes the distance from state  $i$  to state  $j$ , and  $f : [0, \infty) \rightarrow [0, \infty)$  is a monotone decreasing score function. Note that the distances  $\{\Delta_{i,j}\}$  can be obtained via a suitable metric defined on the state space (see subsequent section). The state partitioning structure itself is then determined by the connected components of the induced ddCRP graph (Figure 6). Our joint distribution, visualized in Figure 5c, thus reads as

$$p(\mathbf{a}, \mathbf{c}, \mathcal{G} \mid \mathbf{s}) = p(\mathbf{c}) \prod_{k=1}^{\infty} p_g(g_k \mid \mathbf{s}) \prod_{d=1}^D \pi^\bullet(a_d \mid s_d, g_{\mathbf{z}(\mathbf{c})|s_d}), \quad (9)$$

where  $\mathbf{z}(\mathbf{c})|_s$  denotes the subgoal label of state  $s$  arising from the considered indicator set  $\mathbf{c}$ . In order to highlight the state dependence of the underlying subgoal mechanism, we refer to this model as ddBNIRL-S.

### 3.2.1 THE CANONICAL STATE METRIC FOR SPATIAL SUBGOAL MODELING

The use of the ddCRP as a prior model for the state partitioning in Equation (9) inevitably requires some notion of distance between any two states of the system, in order to compute the involved function scores  $\{f(\Delta_{i,j})\}$ . When no such distances are provided by the problem setting, a suitable (quasi-)metric can be derived from the transition dynamics of the system, which turns out to be the canonical choice for our ddBNIRL-S model. Consider the Markov chain governing the state process  $\{s_{t=n}\}_{n=1}^{\infty}$  of an agent for some specific policy  $\pi$ . For any ordered pair of states  $(i, j)$ , the chain naturally induces a value  $T_{i \rightarrow j}^\pi$ , called a *hitting time* ([Taylor and Karlin, 1984](#); [Tewari and Bartlett, 2008](#)), which represents the expected number of steps required until the state process, initialized at  $i$ , eventually reaches state  $j$  for the first time,

$$T_{i \rightarrow j}^\pi := \mathbb{E}[\min\{n \in \mathbb{N} : s_{t=n} = j\} \mid s_0 = i, \pi].$$

In the context of our subgoal problem, the natural quasi-metric to measure the directed distance between two states  $i$  and  $j$  is thus given by the time it takes to reach the goal state  $j$  from the starting state  $i$  under the corresponding optimal subgoal policy  $\pi_j(s) := \arg \max_{a \in \mathcal{A}} Q^*(s, a \mid j)$ , i.e.,  $\Delta_{i,j} := T_{i \rightarrow j}^{\pi_j}$ . For ddBNIRL-S (as well as for the waypoint method in BNIRL, see Limitation 2), this choice is particularly appealing since the subgoal policies  $\{\pi_j\}$  are already available within the inference procedure (more on this in Section 4.5). The corresponding distances  $\{\Delta_{i,j}\}$  can be computed efficiently in a single policy evaluation step since they correspond to the optimal (negative) expected returns at the starting states for the special setting where the respective target state is made absorbing

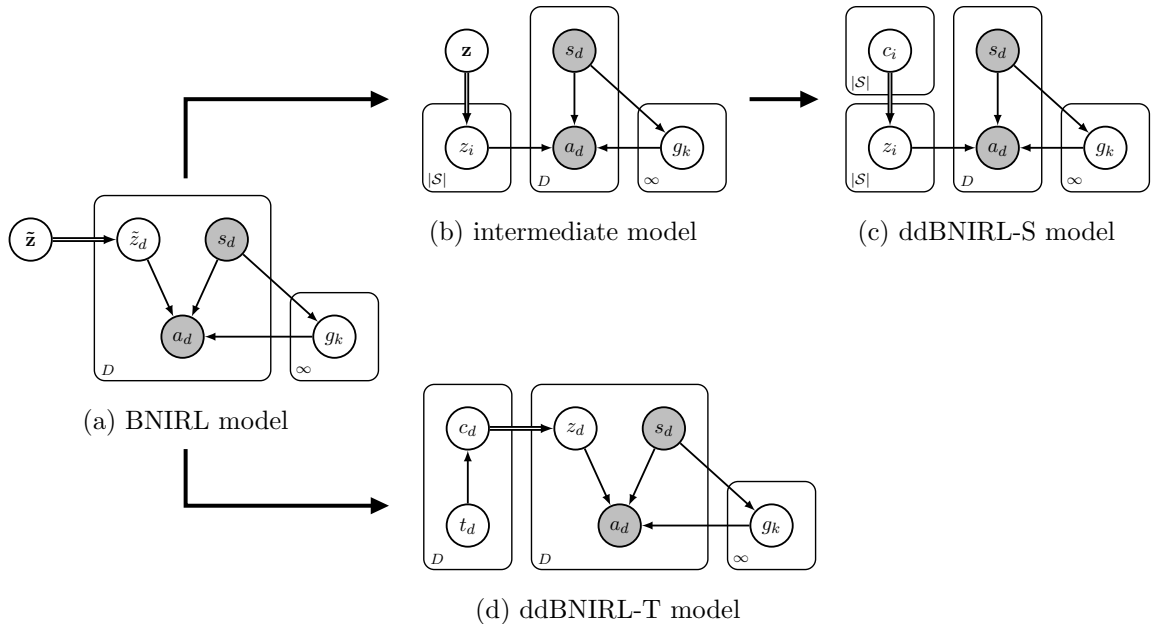


Figure 5: Relationship between the presented model structures, illustrated in the form of Bayesian networks. Shaded nodes represent observed variables, deterministic dependencies are highlighted using double strokes.

with zero reward while all other states are assigned a reward of  $-1$ . Note that, in order to implement a desired degree of locality in the model, the scale of the decay function  $f$  can be further calibrated based on the quantiles of the resulting distribution of distance values.

### 3.3 Modeling Time-Varying Intentions

For the case of changing expert intentions, we need to keep the flexibility of the BNIRL model to select a new subgoal at each decision instant, instead of restricting our policy to target a unique subgoal per state (Figure 3). Hence, we will reuse the basic BNIRL structure and define our subgoal allocation mechanism using a set of data-related indicator variables. However, in contrast to BNIRL, which makes no assumptions about the temporal relationship of the subgoals and allows for arbitrary changes of the expert’s intentions, we design our joint distribution in a way that favors smooth action plans in which the expert persistently follows a subgoal over an extended period of time. Again, we can make use of the ddCRP principle to encode the underlying smoothness assumption, but this time using a score function defined on the *temporal distance* between demonstration pairs. For this purpose, we require an additional piece of information, namely the unique time stamp of each demonstration example. To be precise, we assume our data set to be of the form  $\tilde{\mathcal{D}} := \{(s_d, a_d, t_d)\}_{d=1}^D$ , where  $t_d$  denotes the recording time of the  $d$ th demonstration pair  $(s_d, a_d)$ .<sup>2</sup>

2. Note that the time stamps  $\{t_d\}$  are naturally available in the data set if the demonstrations are recorded in the form of trajectories. In fact, the temporal information of the data is also required for the waypoint

The prior distribution over data partitionings can then be written as  $p(\tilde{\mathbf{c}}) = \prod_{d=1}^D p(\tilde{c}_d)$ ,

$$p(\tilde{c}_d = d') \propto \begin{cases} \nu & \text{if } d = d', \\ f(\tilde{\Delta}_{d,d'}) & \text{otherwise,} \end{cases}$$

where the indices  $d, d' \in \{1, \dots, D\}$  range over the size of the demonstration set. Herein,  $\tilde{\Delta}_{d,d'} := |t_d - t_{d'}|$  denotes the temporal distance between the data points  $d$  and  $d'$ . As before, we use the “ $\sim$ ”-notation to distinguish the data-related partitioning variables  $\tilde{\mathbf{c}}, \tilde{\mathbf{z}}$  and distances  $\{\tilde{\Delta}_{i,j}\}$  from their state space related counterparts  $\mathbf{c}, \mathbf{z}$  and  $\{\Delta_{d,d'}\}$  used in BNIRL and ddbNIRL-S. With that, we obtain our temporal subgoal model as

$$p(\mathbf{a}, \tilde{\mathbf{c}}, \mathcal{G} | \mathbf{s}) = p(\tilde{\mathbf{c}}) \prod_{k=1}^{\infty} p_g(g_k | \mathbf{s}) \prod_{d=1}^D \pi^\bullet(a_d | s_d, g_{\tilde{\mathbf{z}}(\tilde{\mathbf{c}})|_d}), \quad (10)$$

where  $\tilde{\mathbf{z}}(\tilde{\mathbf{c}})|_d$  refers to the subgoal label of the  $d$ th demonstration pair induced by the given assignment  $\tilde{\mathbf{c}}$ . Analogous to our spatial subgoal model, we will refer to this model as ddbNIRL-T. The structural difference between all models can be seen from Figure 5.

### 3.3.1 RELATIONSHIP TO BNIRL

Since the distance-dependent CRP model contains the classical CRP as a special case for a specific choice of distance metric and score function (Blei and Frazier, 2011), the temporal ddbNIRL-T model can be considered a strict generalization of the original BNIRL framework if we neglect the likelihood normalization (Section 3.1). In the same way, the spatial ddbNIRL-S model generalizes the intermediate model presented in Section 3.2 (Figure 5). However, although the BNIRL model can be recovered from ddbNIRL, it is important to note that the sampling mechanisms of both models are fundamentally different. Whereas in BNIRL we sample the subgoal assignments directly, the clustering structure in ddbNIRL is defined *implicitly* via the assignment variables  $\mathbf{c}$  and  $\tilde{\mathbf{c}}$ , respectively. As explained by Blei and Frazier (2011), this has the effect that the Markov Chain underlying the Gibbs sampler mixes significantly faster because several cluster assignments can be altered in a single step, effectively realizing a blocked Gibbs sampler (Roberts and Sahu, 1997).

## 4. Prediction & Inference

Having introduced the ddbNIRL framework, we now explain how it can be used to generalize the expert behavior. To this end, we first focus on the task of action prediction at a given test state, and then explain in a second step how to extract the necessary information from the demonstration data. Along the way, we also give insights into the implicit intentional model learned through the framework.

**Note:** In order to keep the level of redundancy at a minimum, the following considerations are based on the time-invariant ddbNIRL-S model. The results for ddbNIRL-T follow straightforwardly; the only change in the equations is the way the subgoals are referenced.

---

method to work (Michini et al., 2015), even though the authors of BNIRL formally assume to have access to the reduced data set of state-action pairs only.

To obtain the corresponding expressions, we simply replace the assignment variables  $\mathbf{c}$  with  $\tilde{\mathbf{c}}$  and change the cluster definition in Equation (15) to  $\mathcal{C}_k := \{d \in \{1, \dots, D\} : \tilde{\mathbf{z}}(\tilde{\mathbf{c}})|_d = k\}$ . Accordingly, all occurrences of  $\mathbf{z}(\mathbf{c})|_{s^*}$  change to  $\tilde{\mathbf{z}}(\tilde{\mathbf{c}})|_{d^*}$ ,  $\mathbf{z}(\mathbf{c})|_{s_d}$  becomes  $\tilde{\mathbf{z}}(\tilde{\mathbf{c}})|_d$ , and  $s_d \in \mathcal{C}_k$  is replaced with  $d \in \mathcal{C}_k$ .

#### 4.1 Action Prediction

Similar to the work by [Abbeel and Ng \(2004\)](#), we consider the task of predicting an action  $a^* \in \mathcal{A}$  at some query state  $s^* \in \mathcal{S}$  that is optimal with respect to the expert’s *unknown* reward model. However, in contrast to most existing IRL methods, our approach is not based on point estimates of the expert’s reward function but takes into account the entire hypothesis space of reward models, in order to obtain the full posterior predictive policy from the expert data. Mathematically, this task is formulated as computing the predictive action distribution  $p(a^* | s^*, \mathcal{D})$ , which captures the full information about the expert behavior contained in the demonstration set  $\mathcal{D}$ . We start by expanding that distribution with the help of the latent state assignments  $\mathbf{c}$ ,

$$p(a^* | s^*, \mathcal{D}) = \sum_{\mathbf{c} \in \mathcal{S}^{|\mathcal{S}|}} p(a^* | s^*, \mathcal{D}, \mathbf{c}) p(\mathbf{c} | \mathcal{D}).$$

The conditional distribution  $p(a^* | s^*, \mathcal{D}, \mathbf{c})$  can be expressed in terms of the posterior distribution of the subgoal targeted at the query state  $s^*$ ,

$$p(a^* | s^*, \mathcal{D}) = \sum_{\mathbf{c} \in \mathcal{S}^{|\mathcal{S}|}} p(\mathbf{c} | \mathcal{D}) \sum_{i \in \mathcal{S}} p(a^* | s^*, \mathbf{c}, g_{\mathbf{z}(\mathbf{c})|_{s^*}} = i) p(g_{\mathbf{z}(\mathbf{c})|_{s^*}} = i | \mathcal{D}, \mathbf{c}),$$

where we used the fact that the prediction  $a^*$  is conditionally independent of the demonstration set  $\mathcal{D}$  given the state partitioning structure and the corresponding subgoal assigned to  $s^*$  (that is, given  $\mathbf{c}$  and  $g_{\mathbf{z}(\mathbf{c})|_{s^*}}$ ). From the joint distribution in Equation (9), it follows that

$$p(g_k | \mathcal{D}, \mathbf{c}) = \frac{1}{Z_k(\mathcal{D}, \mathbf{c})} p_g(g_k | \mathbf{s}) \prod_{d: \mathbf{z}(\mathbf{c})|_{s_d} = k} \pi(a_d | s_d, g_k), \quad (11)$$

where  $Z_k(\mathcal{D}, \mathbf{c})$  is the corresponding normalizing constant,

$$Z_k(\mathcal{D}, \mathbf{c}) := \sum_{i \in \text{supp}(p_g)} p_g(g_k = i | \mathbf{s}) \prod_{d: \mathbf{z}(\mathbf{c})|_{s_d} = k} \pi(a_d | s_d, g_k = i). \quad (12)$$

Using this relationship, we get

$$\begin{aligned} p(a^* | s^*, \mathcal{D}) &= \sum_{\mathbf{c} \in \mathcal{S}^{|\mathcal{S}|}} \frac{1}{Z_k(\mathcal{D}, \mathbf{c})} p(\mathbf{c} | \mathcal{D}) \sum_{i \in \text{supp}(p_g)} p_g(g_{\mathbf{z}(\mathbf{c})|_{s^*}} = i | \mathbf{s}) \dots \\ &\dots \times \prod_{d: \mathbf{z}(\mathbf{c})|_{s_d} = \mathbf{z}(\mathbf{c})|_{s^*}} \pi(a_d | s_d, g_{\mathbf{z}(\mathbf{c})|_{s^*}} = i) p(a^* | s^*, \mathbf{c}, g_{\mathbf{z}(\mathbf{c})|_{s^*}} = i). \end{aligned}$$

In contrast to the summation over subgoal locations, whose computational complexity is determined by the support of the subgoal prior distribution  $p_g$  and which grows at most

linearly with the size of  $\mathcal{S}$ , the marginalization with respect to the indicator variables  $\mathbf{c}$  involves the summation of  $|\mathcal{S}|^{|\mathcal{S}|}$  terms and becomes quickly intractable even for small state spaces. Therefore, we approximate this operation via Monte Carlo integration, which yields

$$p(a^* | s^*, \mathcal{D}) \approx \frac{1}{N} \sum_{n=1}^N \sum_{i \in \text{supp}(p_g)} p(g_{\mathbf{z}(\mathbf{c}^{\{n\}})|_{s^*}} = i | \mathcal{D}, \mathbf{c}^{\{n\}}) p(a^* | s^*, \mathbf{c}^{\{n\}}, g_{\mathbf{z}(\mathbf{c}^{\{n\}})|_{s^*}} = i),$$

where  $\mathbf{c}^{\{n\}} \sim p(\mathbf{c} | \mathcal{D})$ . The final prediction step can then be performed, for example, via the maximum a posteriori (MAP) policy estimate,

$$\hat{\pi}(s^*) := \arg \max_{a^* \in \mathcal{A}} p(a^* | s^*, \mathcal{D}). \quad (13)$$

The inference task, hence, reduces to the computation of the posterior samples  $\{\mathbf{c}^{\{n\}}\}$ , which is described in the next section.

## 4.2 Partition Inference

Based on the joint model in Equation (9), we obtain the posterior distribution  $p(\mathbf{c} | \mathcal{D})$  in factorized form as

$$\begin{aligned} p(\mathbf{c} | \mathcal{D}) &= p(\mathbf{c}) \prod_{k=1}^{\infty} \sum_{g_k \in \text{supp}(p_g)} p_g(g_k | \mathbf{s}) \prod_{d=1}^D \pi(a_d | s_d, g_{\mathbf{z}(\mathbf{c})|_{s_d}}) \\ &= p(\mathbf{c}) \prod_{k=1}^{|\mathbf{z}(\mathbf{c})|} \sum_{g_k \in \text{supp}(p_g)} p_g(g_k | \mathbf{s}) \prod_{d: s_d \in \mathcal{C}_k} \pi(a_d | s_d, g_k), \end{aligned} \quad (14)$$

where  $\mathcal{C}_k$  denotes the  $k$ th state cluster induced by the assignment  $\mathbf{c}$ ,

$$\mathcal{C}_k := \{s \in \mathcal{S} : \mathbf{z}(\mathbf{c})|_s = k\}, \quad (15)$$

and  $|\mathbf{z}(\mathbf{c})|$  is the total number of clusters defined by  $\mathbf{c}$ . As explained by [Blei and Frazier \(2011\)](#), the indicator samples  $\{\mathbf{c}^{\{n\}}\}$  can be efficiently generated using a fast-mixing Gibbs chain. Starting from a given ddCRP graph defined by the subset of indicators  $\mathbf{c}_{\setminus i} := \{c_j\} \setminus c_i$ , the insertion of an additional edge  $c_i$  will result in one of three possible outcomes, as illustrated in [Figure 6](#): in the case of adding a self-loop ( $c_i = i$ ), the underlying partitioning structure stays unaffected. Setting  $c_i \neq i$  either leaves the structure unchanged (if the target state is already in the same cluster as state  $i$ ) or creates a new link between two clusters. In the latter case, the involved clusters are merged, which corresponds to a merging of the associated sums in Equation (14). According to those three cases, the conditional distribution for the Gibbs procedure is obtained as

$$p(c_i = j | \mathbf{c}_{\setminus i}, \mathcal{D}) \propto \begin{cases} \nu & \text{if } i = j, \\ f(d_{i,j}) & \text{if no clusters are merged,} \\ f(d_{i,j}) \frac{\mathcal{L}(\mathcal{C}_{z_i} \cup \mathcal{C}_{z_j})}{\mathcal{L}(\mathcal{C}_{z_i}) \cdot \mathcal{L}(\mathcal{C}_{z_j})} & \text{if clusters } \mathcal{C}_{z_i} \text{ and } \mathcal{C}_{z_j} \text{ are merged.} \end{cases} \quad (16)$$

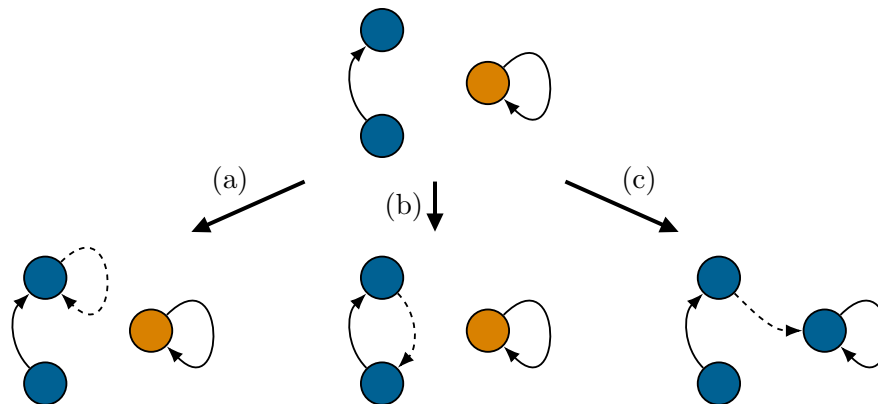


Figure 6: Insertion of an edge (dashed arrow) in the ddCRP graph. The colors indicate the cluster membership of the nodes, which is defined implicitly via the connected components of the graph. (a) Adding a self-loop or (b) adding an edge between two already connected nodes does not change the clustering structure. (c) Adding an edge between two unconnected components merges their clusters.

Herein,  $\mathcal{L}(\mathcal{C})$  denotes the marginal action likelihood of all demonstrations accumulated in cluster  $\mathcal{C}$ ,

$$\mathcal{L}(\mathcal{C}) = \sum_{g \in \text{supp}(p_g)} p_g(g | \mathbf{s}) \prod_{d: s_d \in \mathcal{C}} \pi(a_d | s_d, g), \quad (17)$$

which further corresponds to the normalizing constant for the posterior distribution of the cluster subgoal (Equation 12). Accordingly, the fraction in Equation (16) can be interpreted as the likelihood ratio of the partitioning defined by  $\mathbf{c}_i$  and the merged structure after inserting the new edge  $c_i$ .

### 4.3 Subgoal Inference

It is important to note that the inference method described in the previous two sections is based on a collapsed sampling scheme where all subgoals of our model are marginalized out. In fact, the ddBNIRL framework differs from BNIRL and other IRL methods in that the reward model of the expert is never made explicit for predicting new actions. Nonetheless, if desired (e.g., for the purpose of analyzing the expert’s intentions), an estimate of the subgoal locations can be obtained in a post-hoc fashion from the subgoal posterior distribution in Equation (11) for any given assignment  $\mathbf{c}$ . Examples of this are provided in Figure 7.

### 4.4 Action Inference

As mentioned in Section 2.2, the original BNIRL algorithm requires complete knowledge of the expert’s action record  $\mathbf{a}$ , which limits the range of potential applications. For this reason, we generalize our inference scheme to the case where we have access to state information only, provided in the form of an alternative data set  $\bar{\mathcal{D}} := \{(s_d, \bar{s}_d)\}_{d=1}^D$ , where  $\bar{s}_d$  refers to the state visited by the expert immediately after  $s_d$ . In this setting, inference can be

performed by extending the Gibbs procedure with an additional collapsed sampling stage,

$$p(a_d | \mathbf{a}_{\setminus d}, \bar{D}, \mathbf{c}) \propto T(\bar{s}_d | s_d, a_d) \sum_{i \in \text{supp}(p_g)} p_g(g_{\mathbf{z}(\mathbf{c})|s_d} = i) \prod_{d': \mathbf{z}(\mathbf{c})|s_{d'} = \mathbf{z}(\mathbf{c})|s_d} \pi(a_{d'} | s_{d'}, g_{\mathbf{z}(\mathbf{c})|s_{d'}} = i), \quad (18)$$

which, for a fixed assignment  $\mathbf{c}$ , recovers the latent action information  $\mathbf{a}$  from the observed state transitions. Note that knowledge of the transition model  $T$  is required for this step as it provides the necessary link between the expert actions and the observed successor states. The same extension is possible for the ddbNIRL-T model, provided that the transition time stamps  $\{t_d\}$  are known (Section 3.3).

#### 4.5 Computational Complexity

As a last point in this section, we would like to discuss the computational complexity of our approach. For this purpose, here a quick reminder on the notation: we write  $|\mathcal{S}|$  and  $|\mathcal{A}|$  for the size of the state and action space, respectively, and use the letter  $D$  for the size of the demonstration set. Further, we write  $\mathcal{C}_k$  to refer to the  $k$ th state cluster (ddbNIRL-S) or data cluster (ddbNIRL-T). In the subsequent paragraphs, we additionally use the notation  $N_D(\mathcal{C}_k)$  to access the number of demonstration data points associated with cluster  $\mathcal{C}_k$ ,  $K$  to indicate the number of clusters in the current iteration,  $N_g := |\text{supp}(p_g)|$  as a shorthand for the size of the support of the subgoal prior distribution, and  $N_c$  for the number of indicator variables, i.e.,  $N_c := |\mathcal{S}|$  for ddbNIRL-S and  $N_c := D$  for ddbNIRL-T.

*Initialization Phase:* Common to all discussed models (including BNIRL) is that they depend on a preceding planning phase, where we compute—in parallel—the state-action value functions (Equation 3) for all  $N_g$  considered subgoals, in order to construct the action likelihood model (Equation 2 or 8, respectively). The overall computational complexity of this procedure is hence of order  $\mathcal{O}(N_g \mathcal{C}_{\text{MDP}}(|\mathcal{S}|, |\mathcal{A}|))$ , where  $\mathcal{C}_{\text{MDP}}(x, y)$  denotes the complexity of the used planning routine to (approximately) solve an MDP of size  $x$  with a total number of  $y$  actions. Using a value iteration algorithm, for instance, this is done in  $\mathcal{O}(\mathcal{C}_{\text{MDP}}(|\mathcal{S}|, |\mathcal{A}|)) = \mathcal{O}(|\mathcal{S}|^2 |\mathcal{A}|)$  steps (Littman et al., 1995). If we assume that the expert reaches all subgoals during the demonstration phase (Michini and How, 2012), we can restrict the support of the subgoal prior to the visited states, so that  $N_g$  is upper bounded by  $\min(|\mathcal{S}|, D)$ . Note that there exist approximation techniques that make the computation tractable in large/continuous state spaces (see discussion in Section 6).

Before we start the sampling procedure, we compute all single-cluster likelihoods  $\{\mathcal{L}(\mathcal{C}_k)\}$  and pairwise likelihoods  $\{\mathcal{L}(\mathcal{C}_k \cup \mathcal{C}_{k'})\}$  according to Equation (17), based on some (random) initial cluster structure. The likelihood computation for the  $k$ th cluster  $\mathcal{C}_k$  involves a product over  $N_D(\mathcal{C}_k)$  data points, which needs to be calculated for each of the  $N_g$  subgoals before taking their weighted average. This step has to be executed (potentially in parallel) for all clusters. However, because each demonstration is associated with exactly one cluster (either directly as in ddbNIRL-T or via the corresponding state variable as in ddbNIRL-S) so that  $\sum_k N_D(\mathcal{C}_k) = D$ , the total complexity for computing all single-cluster likelihoods is of order  $\mathcal{O}(N_g D)$ , irrespective of the cluster structure. A similar line of reasoning applies to the computation of the pairwise likelihoods, yielding the same complexity order. Yet, for the latter we need to consider all possible cluster combinations. Assuming an initial

number of  $K$  clusters, there are in total  $K(K - 1)/2$  pairwise likelihoods to be computed. Hence, the overall complexity of the initialization phase can be summarized as  $\mathcal{O}(N_gDK^2)$ .

*Partition Inference:* For the partition inference, the bulk of the computation lies in the repeated construction of the likelihood term in Equation (16), which needs to be updated whenever the cluster structure changes. To analyze the complexity, we consider the sampling step of an individual assignment variable  $c_i$  (or similarly  $\tilde{c}_i$ ). In the worst case, removing the edge that belongs to  $c_i$  in the ddCRP graph will divide the associated cluster into two parts (Figure 6), so that two new single-cluster likelihoods need to be computed. With the upper bound  $D$  on the number of data points associated with the cluster before the division, this operation is of worst-case complexity  $\mathcal{O}(N_gD)$  (see initialization phase). Irrespective of whether a division occurs, we then need to compute all pairwise cluster likelihoods that involve the (new) cluster tied to  $c_i$ . For a total of  $K - 1$  possible choices, this is done in  $\mathcal{O}(N_gDK)$  operations (see previous paragraph again). After assigning the indicator, we move on to the next variable where the process repeats. If we assume, for simplicity, that the number of clusters stays constant during a full Gibbs cycle, the total complexity of updating all cluster assignments is hence of order  $\mathcal{O}(N_gDKN_c)$ . A (pessimistic) upper bound for the general case can be obtained by assuming that each data point defines its own cluster, in which case we get  $\mathcal{O}(N_gD^2N_c)$ . Note that, in order to identify the new set of clusters after changing an assignment, we additionally need to track the connected components of the underlying ddCRP graph. As explained by [Kapron et al. \(2013\)](#), this can be done in polylogarithmic worst-case time.

*Action Sampling:* In order to compute the conditional probability distribution of a particular action  $a_d$ , we need to evaluate a product involving all actions that belong to the same cluster as  $a_d$  (Equation 18). First, we compute the product over all actions except  $a_d$  itself, where the number of involved terms is again upper bounded by  $D$ . Appending the term that belongs to  $a_d$  for all possible action choices requires another  $|\mathcal{A}|$  operations. These two steps need to be repeated for all possible subgoals, yielding an upper bound on the complexity of order  $\mathcal{O}(N_g(D + |\mathcal{A}|))$ . For a full Gibbs cycle, which involves sampling all  $D$  action variables, the overall (worst-case) complexity is hence of order  $\mathcal{O}(N_g(D + |\mathcal{A}|)D)$ .

## 5. Experimental Results

In this section, we present experimental results for our algorithm, which we separate into four parts: (i) a proof of concept and conceptual comparison to BNIRL, (ii) a performance comparison with related algorithms, (iii) a real data experiment conducted on a KUKA robot and (iv) an active learning task.

### 5.1 Proof of Concept

To illustrate the conceptual differences to BNIRL and provide empirical insights into the latent intentional model learned through our framework, we begin with one of the data sets presented in the original BNIRL paper ([Michini and How, 2012](#)). The considered system environment, defined by  $|\mathcal{S}| = 20 \times 20 = 400$  grid positions, is shown in the top left corner of Figure 7. Nine of those grid positions correspond to inaccessible wall states, marked

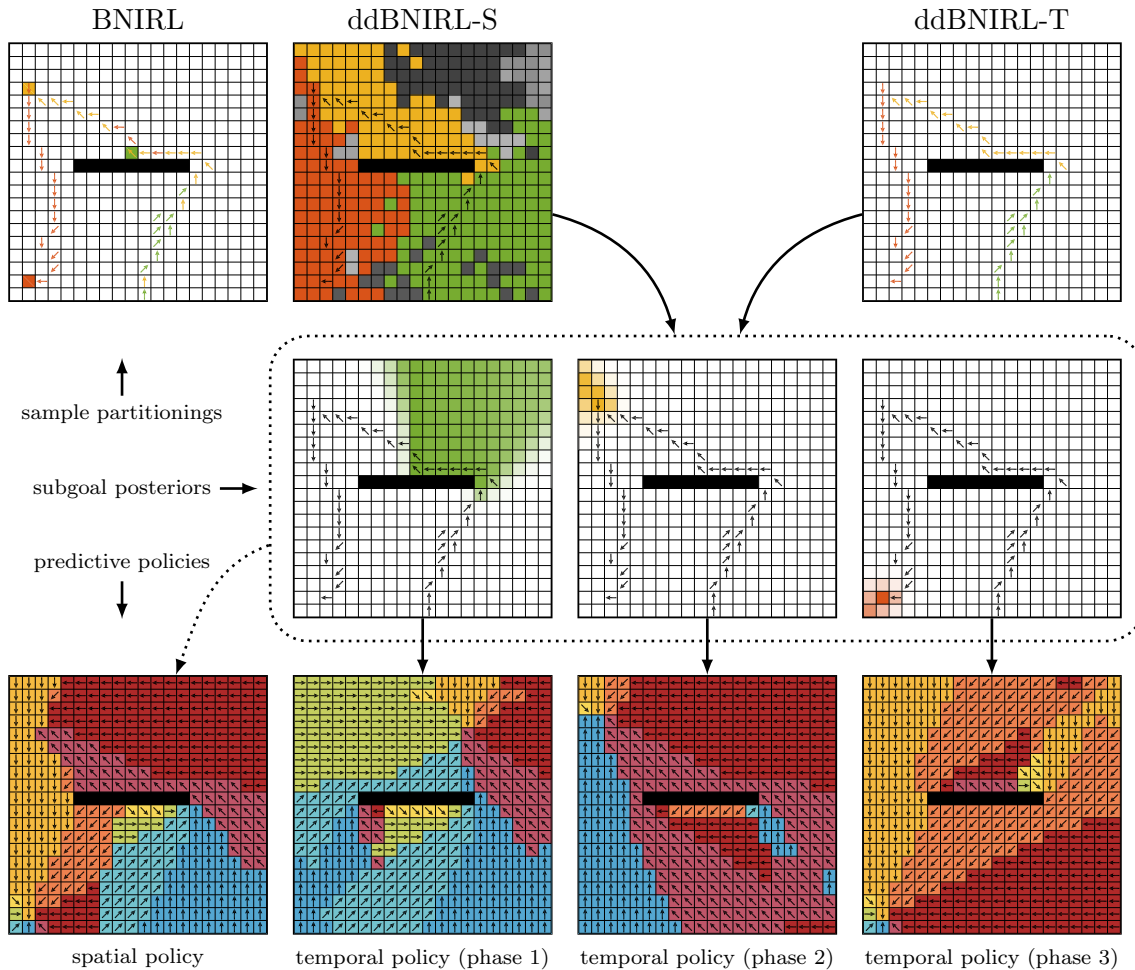


Figure 7: Results on the BNIRL data set (Michini and How, 2012). **Top row:** demonstration data and sample partitionings generated by the inference algorithms. **Center row:** subgoal posterior distributions corresponding to the partitions found by ddBNIRL-S and ddBNIRL-T. For space reasons, we omit the BNIRL distributions (see Figure 4 for a comparison). **Bottom row:** time-invariant ddBNIRL-S policy model synthesized from all three detected subgoals and the temporal phases identified by ddBNIRL-T. Because of the missing generalization mechanism, BNIRL does itself not provide a policy model (Limitation 1).

by the black horizontal bar. At each of the valid states, the expert can choose from an action set comprising a total of eight actions, each initiating a noisy state transition toward one of the (inter-)cardinal directions. The observed state-action pairs are depicted in the form of arrows, whose colors indicate the MAP partitioning learned through BNIRL. The remaining subfigures show the results of the ddBNIRL framework, which we computed from a posterior sample returned by the respective algorithm (ddBNIRL-S/T) at a low temperature in a simulated annealing schedule (Kirkpatrick et al., 1983).

Comparing the obtained results, we observe the following main differences to the original approach: (i) unlike BNIRL, the proposed framework allows us to choose between a temporal and a spatial encoding of the demonstrated task, in order to explicitly account for the type of demonstrated behavior (time-varying/time-invariant). As explained in Section 3.3.1, the context-unaware—yet in principle temporal—vanilla BNIRL inference scheme is still included as a special case. (ii) Exploiting the spatial/temporal context of the data, the ddBNIRL solution is inherently robust to demonstration noise, giving rise to notably smoother partitioning structures (top row). This effect is particularly pronounced in the case of real data, as we shall see later in Section 5.3.2. (iii) For each state partition/trajectory segment, we obtain an implicit representation of the associated subgoal in the form of a posterior distribution, without the need of assigning point estimates (center row). It is striking that the posterior distribution corresponding to the green state partition has a comparably large spread on the upper side of the wall. This can be explained intuitively by the fact that any subgoal located in this high posterior region could have potentially caused the green state sequence, which circumvents the wall from the right. At the same time, the green area of high posterior values exhibits a sharp boundary on the left side since a subgoal located in the upper left region of the state space would have more likely resulted in a trajectory approaching from the left. (iv) In contrast to BNIRL, which has no built-in generalization mechanism (Limitation 1), our method returns a predictive policy model comprising the full posterior action information at all states. Note that we only show the resulting MAP policy estimates here (bottom row), computed according to Equation (13); additional results regarding the posterior uncertainty are shown later in Section 5.3. The example illustrates how the synthesis of the predictive model differs between ddBNIRL-S (leftmost subfigure) and ddBNIRL-T (rightmost three subfigures). While ddBNIRL-T uses a set of (conditionally) independent policy models to describe the different identified behavioral phases, ddBNIRL-S maps the entire subgoal schedule onto a single time-invariant policy representation. Looking closer at the learned models, we recognize that the ddBNIRL-S solution in fact realizes a spatial combination of the three temporal ddBNIRL-T components, where each phase is activated in the corresponding cluster region of the state space. This provides us two alternative explanations of the same task.

## 5.2 Random MDP

Our next experiment is designed to provide insights into the generalization abilities of the framework. For this purpose, we consider a class of randomly generated MDPs, similar to the Garnet setting (Bhatnagar et al., 2009). The transition dynamics  $\{T(\cdot | s, a)\}$  are sampled independently from a symmetric Dirichlet distribution with concentration parameter 0.01, where we set  $|\mathcal{S}| = 100$  and  $|\mathcal{A}| = 10$ . For each repetition of the experiment,  $N_R$  states are selected uniformly at random and assigned rewards that are, in turn, sampled uniformly from the interval  $[0, 1]$ . All other states contain zero reward. Next, we compute an optimal deterministic policy  $\pi^*$  with respect to a discount factor of  $\gamma = 0.9$  and generate a number of expert trajectories of length 10. Herein, we let the expert select the optimal action with probability 0.9 and a random, suboptimal action with probability 0.1. The obtained state sequences are passed to the different algorithms and we compute the normalized value loss

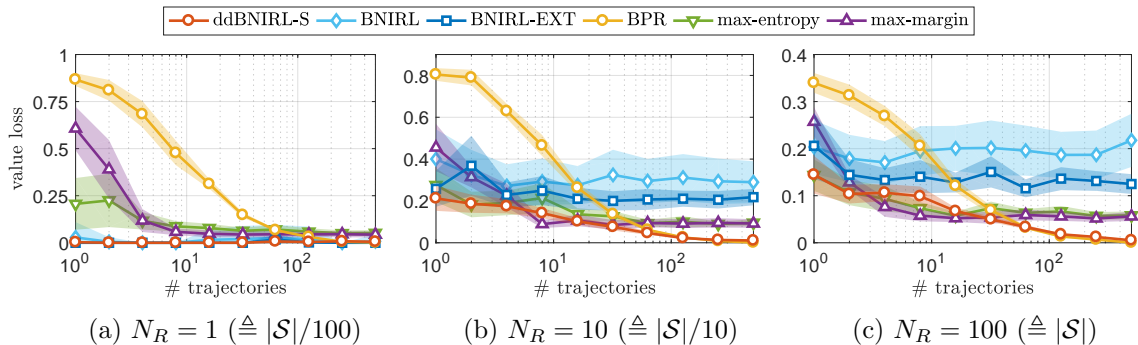


Figure 8: Average value loss in the random MDP scenario based on 100 Monte Carlo runs. The width of the shaded areas indicates one standard deviation.

of the reconstructed policies according to

$$L(\pi^*, \hat{\pi}) := \frac{\|\mathbf{V}^* - \mathbf{V}^{\hat{\pi}}\|_2}{\|\mathbf{V}^*\|_2}, \quad (19)$$

where  $\mathbf{V}^*$  and  $\mathbf{V}^{\hat{\pi}}$  represent the vectorized value functions of the optimal policy  $\pi^*$  and the reconstruction  $\hat{\pi}$ , respectively.

Since the considered system belongs to the class of MDPs with time-invariant reward functions, ddBNIRL-S lends itself as the natural choice to model the expert behavior. As baseline methods, we adopt the subintentional Bayesian policy recognition framework (Šošić et al., 2018b), as well as maximum-margin IRL (Abbeel and Ng, 2004), maximum-entropy IRL (Ziebart et al., 2008), and vanilla BNIRL. Due to the missing generalization abilities of BNIRL (Limitation 1) and because the waypoint method (Section 2.2) does not straightforwardly apply to the considered scenario of multiple unaligned trajectories, we further compare our algorithm to an extension of BNIRL, which we refer to as BNIRL-EXT. Mimicking the ddBNIRL-S principle, the method accounts for the spatial context of the demonstrations by assigning each state to the BNIRL subgoal targeted by the closest (see Section 3.2.1) state-action pair—however, these assignments are made *after* the actual subgoal inference. When compared to ddBNIRL-S, this provides a reference of how much is effectively gained by modeling the spatial relationship of the data explicitly. For the experiment, both ddBNIRL-S and BNIRL(-EXT) are augmented with their corresponding action sampling stages (Section 4.4) since the action sequences of the expert are discarded from the data set, in order to enable a fair comparison to the remaining algorithms.

Figure 8 shows the value loss over the size of the demonstration set for different reward settings. For small  $N_R$ , both BNIRL(-EXT) and ddBNIRL-S significantly outperform the reference methods. This is because the sparse reward structure allows for an efficient subgoal-based encoding of the expert behavior, which enables the algorithms to reconstruct the policy from even minimal amounts of demonstration data. However, the BNIRL(-EXT) solutions drastically deteriorate for denser reward structures. In particular, we observe a clear difference in performance between the cases where (i) we do not account for the spatial information at all (BNIRL), (ii) include it in a post-processing step (BNIRL-EXT), and (iii) exploit it during the inference itself (ddBNIRL-S), which demonstrates the importance of

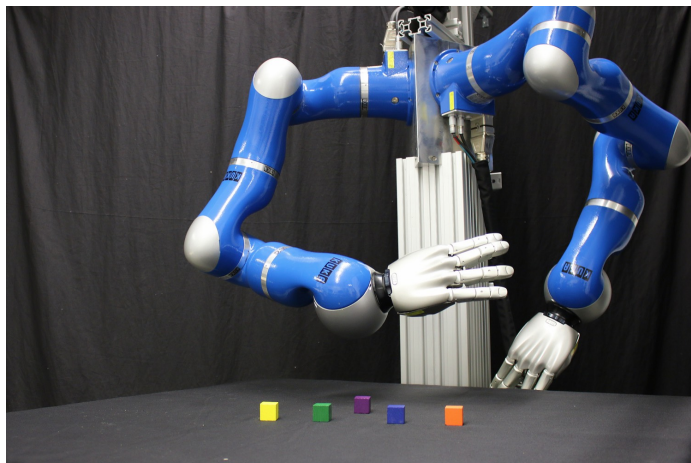


Figure 9: KUKA leightweight arm.

processing the context information. Most tellingly, ddBNIRL-S outperforms the baseline methods even in the dense reward regimes, although the subgoal-based encoding loses its efficiency here. In fact, the results reveal that the proposed approach combines the merits of both model types, i.e., the sample efficiency of the intentional models (max-margin/max-entropy) required for small data set sizes, as well as the asymptotic accuracy and fully probabilistic nature of the subintentional Bayesian framework (BPR).<sup>3</sup>

### 5.3 Robot Experiment

In the next experiment, we test the ddBNIRL framework on various real data sets, which we recorded on a KUKA lightweight arm (Figure 9) via kinesthetic teaching. Videos of all demonstrated tasks can be found in the supplementary material.

The system has seven degrees of freedom, corresponding to the seven joints of the arm. Each joint is equipped with a torque sensor and an angle encoder, providing recordings of joint angles, velocities and accelerations. For our experiments, only the xy-Cartesian coordinates spanning the transverse plane are considered, which we computed from the raw measurements using a forward kinematic model. The data was recorded at a sampling rate of 50 Hz and further downsampled by a factor of 10, yielding an effective sample rate of 5 Hz, which provided a sufficient temporal resolution for the considered scenario.

The goal of the experiments is to learn a set of high-level intentional models for the recorded behaviors by partitioning the data sets into meaningful parts that can be used to predict the desired motion direction of the expert. For simplicity, and to demonstrate the algorithm’s robustness to modeling errors, we adopt the simplistic transition model from Section 5.1 with the same action set containing the eight (inter-)cardinal motion directions. The high measurement accuracy of the end-effector position allows us to extract these high-level actions directly from the raw data, i.e., by selecting the directions with the

---

3. The comparably large loss of BPR for small data set sizes can be explained by the fact that BPR is based on a more general policy model in which the expert behavior is assumed to be *inherently* stochastic, in contrast to the considered setting where stochasticity arises merely a consequence of suboptimal control.

smallest angular deviations from the ground truth. The underlying state space is obtained by discretizing the part of the coordinate range that is covered by the measurements into blocks of predefined size (see next sections for details). Apart from this discretization step and the mentioned downsampling, no preprocessing is applied.

### 5.3.1 SPATIAL PARTITIONING

First, we consider a case where the expert behavior can be described using a time-invariant policy model, which we aspire to capture via ddBNIRL-S. For our example, we consider the “Cycle” task shown in the video. The same setting is later analyzed using the time-variant ddBNIRL-T model, which allows a direct comparison of the two approaches (Section 5.3.2). The task consists in approaching a number of target positions, indicated by a set of markers (see video), before eventually returning to the initial state. The setting can be regarded as a real-world version of the “Loop” problem described by Michini and How (2012). As explained in their paper, classical IRL algorithms that use a holistic state-based reward model (such as max-margin and max-entropy) completely fail on this problem, due to the periodic nature of the task.

Figure 10a shows the recorded data set (black arrows) obtained from four expert trajectories (white lines). For visualization purposes, the discretization block size is chosen as  $2\text{ cm} \times 2\text{ cm}$ , giving rise to a total of  $18 \times 24 = 432$  states. As in Figure 7, the coloring of the background indicates the learned partitioning structure, computed from a low-temperature posterior sample. We observe that the found state clusters clearly reveal the modular structure of the task, providing an intuitive and interpretable explanation of the data. However, though the induced policy model (Figure 10b) smoothly captures the cyclic nature of the task, we cannot expect to obtain trustworthy predictions in the center region of the state space, due to the lack of additional demonstration data that would be required to unveil the expert’s true intention in that region. Clearly, a point estimate such as the shown MAP policy cannot reflect this prediction uncertainty since it does not carry any confidence information. Yet, following a Bayesian approach, we can naturally quantify the prediction uncertainty at any query state  $s^*$  based on the posterior predictive distribution  $p(a^* | s^*, \mathcal{D})$ . A straightforward option is, for example, to consider the prediction entropy,

$$H(s^*) := \sum_{a^* \in \mathcal{A}} p(a^* | s^*, \mathcal{D}) \log p(a^* | s^*, \mathcal{D}).$$

To obtain an unbiased approximation of the true *non-tempered* predictive distribution  $p(a^* | s^*, \mathcal{D})$ , we run a second Gibbs chain with unaltered temperature in parallel to the tempered chain. The the resulting entropy estimates are summarized in an uncertainty map (Figure 10c), which we overlaid with the original prediction result to produce the final figure shown on the bottom right. Note that the obtained posterior uncertainty information of the model can be further used in an active learning setting, as will be demonstrated in Section 5.4.

### 5.3.2 TEMPORAL PARTITIONING

Next, we focus our attention on the ddBNIRL-T model, which we test against the vanilla BNIRL approach. For this purpose, we consider the full collection of tasks shown in the

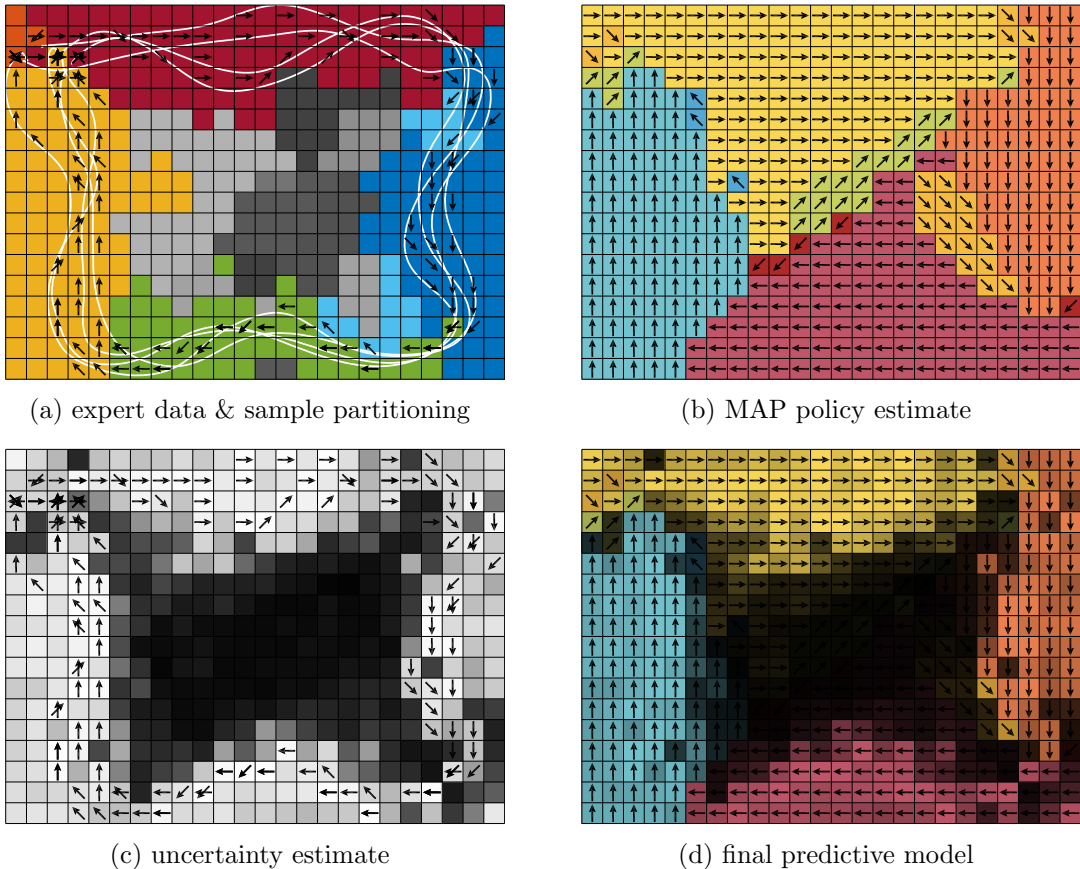


Figure 10: Result of ddBNIRL-S on the “Cycle” task. (a) Raw measurements (white lines) and discretized demonstration data (black arrows). The coloring of the background indicates a partitioning structure obtained from a low-temperature posterior sample. (b) Maximum a posteriori policy estimate returned by the model. (c) Visualization of the prediction uncertainty based on the entropy of the predictive action distribution. (d) Illustration of the final predictive model, comprising both the action information and the prediction uncertainty.

supplementary video, which comprises different time-dependent expert behaviors of varying complexity. In order to obtain a quantitative performance measure for our evaluation, we conducted a manual segmentation of all recorded trajectories, thereby producing a set of ground truth subgoal labels for all observed decision instants. The result of this segmentation step is depicted in the appendix (Figure 13, center column). Note that the ground truth subgoals are assumed to be located immediately at the ends of the shown segments.

The left and right column of Figure 13 show, respectively, the partitioning structures found by BNIRL and ddBNIRL-T, based on a uniform subgoal prior distribution with support at the visited states. The underlying state discretization block size is chosen as  $1\text{ cm} \times 1\text{ cm}$ , as indicated by the regular grid in the background. A simple visual comparison of the learned structures reveals the clear superiority of ddBNIRL-T over vanilla BNIRL on

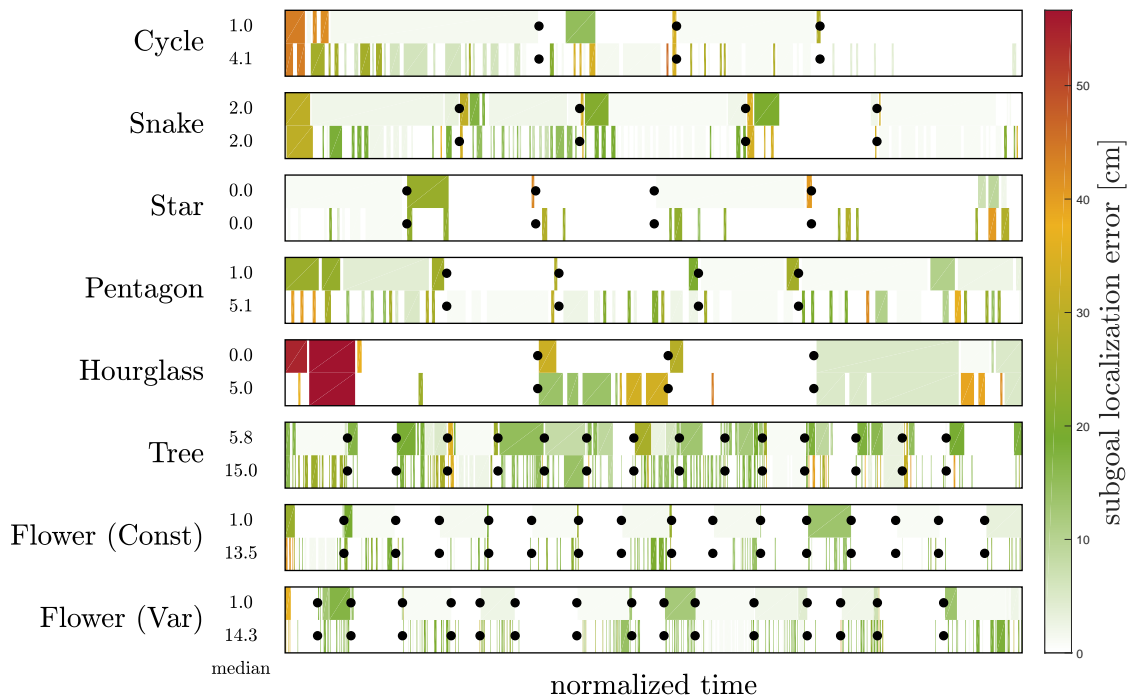


Figure 11: Subgoal localization errors of ddbNIRL-T (top rows) and BNIRL (bottom rows) for the demonstrated tasks shown in the supplement, measured in Euclidean distance. The black dots indicate a change in the ground truth subgoal annotation.

this problem. For a quantitative comparison, we show the instantaneous subgoal prediction errors of the two models in the Euclidean space in Figure 11. For ddbNIRL-T, which does not directly return a subgoal location estimate but instead provides access to the full subgoal posterior distribution, the error is computed with respect to the MAP subgoal locations,

$$\hat{g}_k := \arg \max_{g_k \in \text{supp}(p_g)} p(g_k | \mathcal{D}, \tilde{\mathbf{c}}),$$

using the ddbNIRL-T version of Equation (11) (see remark at the beginning of Section 4). The black dots in the figure indicate the time instants where the ground truth annotations change. At those time instants, we observe significantly increased localization errors, which can be explained by the fact that the assumed ground truth annotation is somewhat subjective around the transition points (see labeling in Figure 13). Also, we notice a comparably high error at the beginning and the end of some trajectories, which stems from the imperfect synchronization between the recording interval and the execution of the task (recall that we skipped the corresponding data preprocessing step). To capture the accuracy in a single figure of performance, we hence consider the median localization error of each time series, as it masks out the outliers and thus provides a more realistic error quantification than the sample mean. The obtained values are shown next to the error plots in Figure 11, indicating that the ddbNIRL-T localization error is in the range of the discretization interval in most

cases. Compared to *BNIRL*, the proposed method yields an error reduction of more than 70% on average.

#### 5.4 Active Learning

In Section 5.3, we saw that the posterior predictive action distribution  $p(a^* | s^*, \mathcal{D})$  provides a natural way to quantify the prediction uncertainty of our model at any given query state  $s^*$ . This offers the opportunity to apply the framework in an active learning setting, since the induced uncertainty map (Figure 10c) indicates in which parts of the state space the trained model can most effectively process further instructions from the expert.

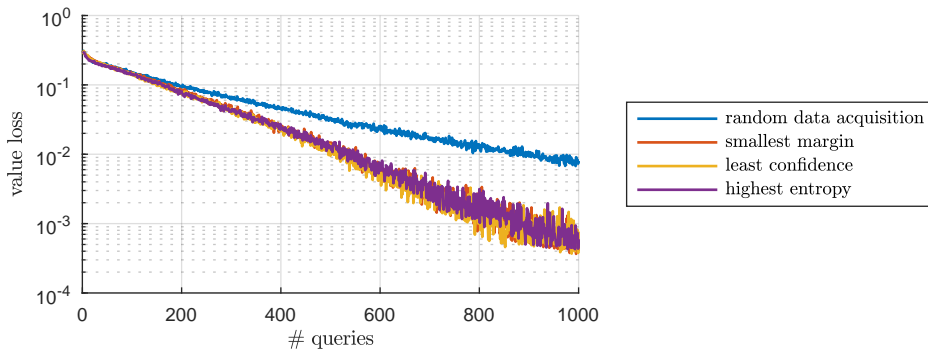


Figure 12: Comparison between random data acquisition and active learning, based on 200 Monte Carlo runs. The curves show the mean value losses of the obtained policy models over the number of data queries.

To demonstrate the basic procedure, we reconsider the random MDP problem from Section 5.2 in an active learning context, where we compare different active learning strategies with the previously used random data acquisition scheme. As an initialization for the learning procedure, we request a single state-action pair  $(s_1, a_1)$  from the demonstrator, which we store in the initial data set  $\mathcal{D}_1 := \{(s_1, a_1)\}$ . Herein, the state  $s_1$  is drawn uniformly at random from  $\mathcal{S}$  and the action  $a_1 \sim \pi_E(a | s_1)$  is generated according to the *true* expert policy  $\pi_E : \mathcal{A} \times \mathcal{S} \rightarrow [0, 1]$ . Continuing from this point, each of the considered active learning algorithms requests a series of subsequent demonstrations  $((s_2, a_2), (s_3, a_3), \dots)$ , inducing a sequence of data sets  $(\mathcal{D}_1, \mathcal{D}_2, \mathcal{D}_3, \dots)$ , where the next query state  $s_{d+1}$  is chosen according to the specific data acquisition criterion  $f_{\text{acq}}$  of the algorithm evaluated on the current predictive model,

$$\begin{aligned} \mathcal{D}_d &= \mathcal{D}_{d-1} \cup \{(s_{d+1}, a_{d+1})\} \\ s_{d+1} &= \arg \max_{s^* \in \mathcal{S}} f_{\text{acq}}[p(a^* | s^*, \mathcal{D}_d)] \\ a_{d+1} &\sim \pi_E(a | s_{d+1}). \end{aligned}$$

The purpose of the acquisition criterion is to assess the uncertainty of the model at all possible prediction states, so that the next demonstration can be requested in the high

uncertainty region of the state space (see *uncertainty sampling*, Settles, 2010). For our experiment, we consider the following three common choices,

- highest entropy:  $f_{\text{acq}}(p) := - \sum_{a \in \mathcal{A}} p(a) \log p(a)$ ,
- least confidence:  $f_{\text{acq}}(p) := 1 - \max_{a \in \mathcal{A}} p(a)$ ,
- smallest margin:  $f_{\text{acq}}(p) := p(\hat{a}_2) - p(\hat{a}_1)$ ,

where  $\hat{a}_1$  and  $\hat{a}_2$  are, respectively, the most likely and second most likely action according to the considered distribution  $p$ , i.e.,  $\hat{a}_1 := \arg \max_{a \in \mathcal{A}} p(a)$  and  $\hat{a}_2 := \arg \max_{a \in \mathcal{A} \setminus \hat{a}_1} p(a)$ . At each iteration, we compute the value losses (Equation 19) of the induced policy models and compare them with the loss that results from random data acquisition. The resulting curves are delineated in Figure 12. As expected, the learning speed of the model is significantly improved under all active acquisition schemes, which reduces the required number of expert demonstrations to successfully learn the observed task.

## 6. Conclusion

Building upon the idea of Bayesian nonparametric inverse reinforcement learning, we proposed a new framework for data-efficient IRL that leverages the context information of the demonstration set to learn a predictive model of the expert behavior from small amounts of training data. Central to our framework are two model architectures, one designed for learning spatial subgoal plans, the other to capture time-varying intentions. In contrast to the original BNIRL model, both architectures explicitly consider the covariate information contained in the demonstration set, giving rise to predictive models that are inherently robust to demonstration noise. While the original BNIRL model can be recovered as a special case of our framework, the conducted experiments show a drastic improvement over the vanilla BNIRL approach in terms of the achieved subgoal localization accuracy, which stems from both an improved likelihood model and the context-aware clustering of the data. Most notably, our framework outperforms all discussed reference methods in the analyzed benchmark scenarios while additionally capturing the full posterior information about the learned subgoal representation. The resulting prediction uncertainty about the expert behavior, reflected by the posterior predictive action distribution, provides a natural basis to apply our method in an active learning setting where the learning system can request additional demonstration data from the expert.

The current limitation of our approach is that both presented architectures require an MDP model with discrete state and action space. While the subgoal principle carries over straightforwardly to continuous metric spaces, the construction of the likelihood model becomes difficult in these environments as it requires knowledge of the optimal state-action value functions for all potential subgoal locations. However, for BNIRL, there exist several ways to approximate the likelihood in these cases (Michini et al., 2013) and the same concepts apply equally to ddBNIRL. Thus, an interesting future study would be to compare the efficacy of both model types on larger problems involving continuous spaces, where it comes even more natural to follow a distance-based approach.

Appendix A. Robot experiment

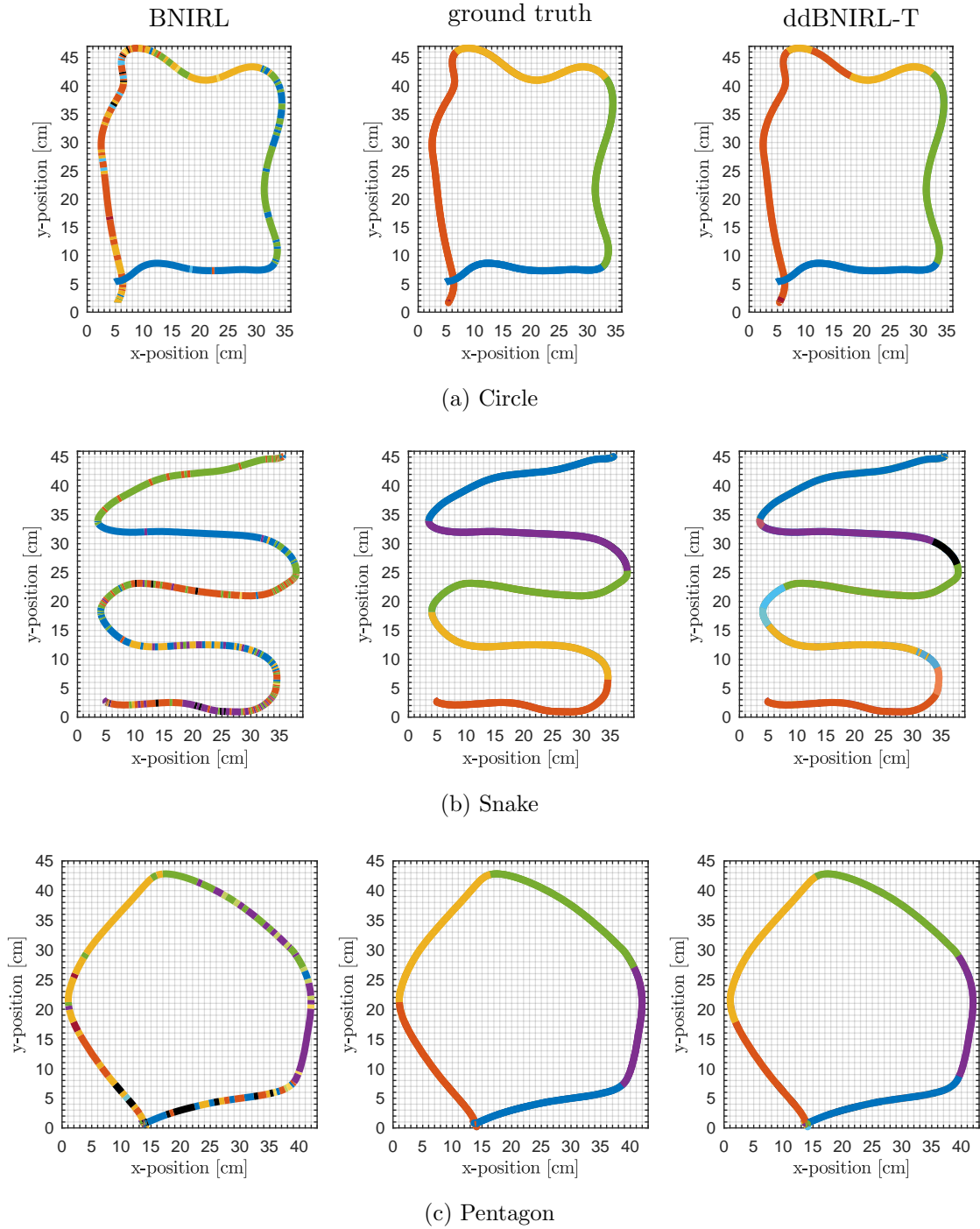


Figure 13: Motion sequences without trajectory crossings, which can be represented using a spatial subgoal pattern.

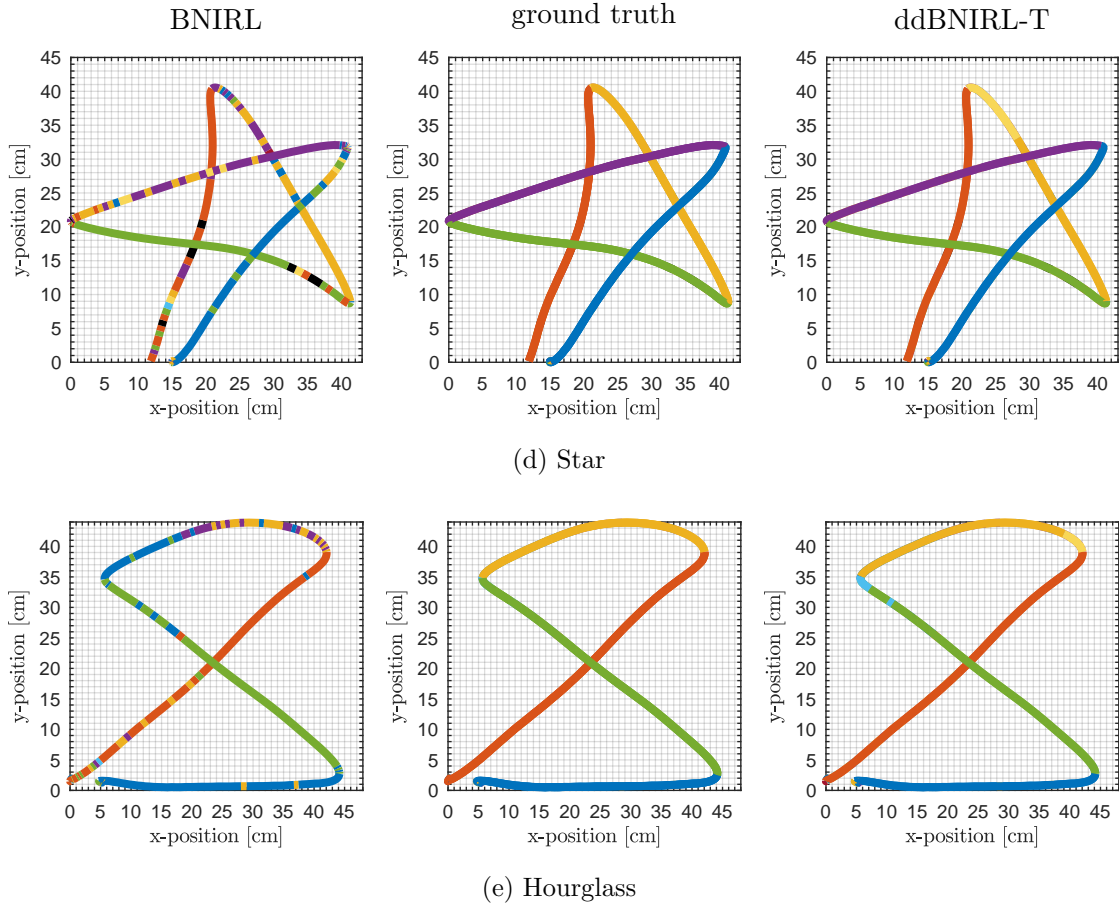
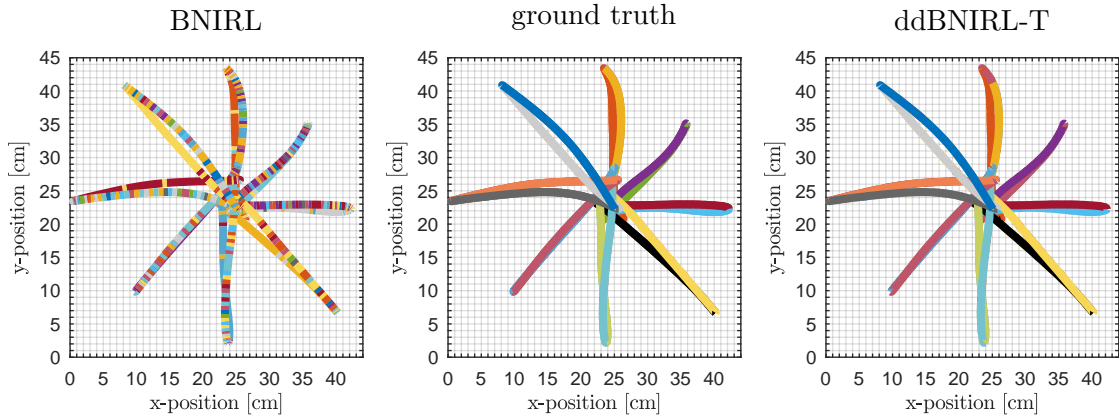
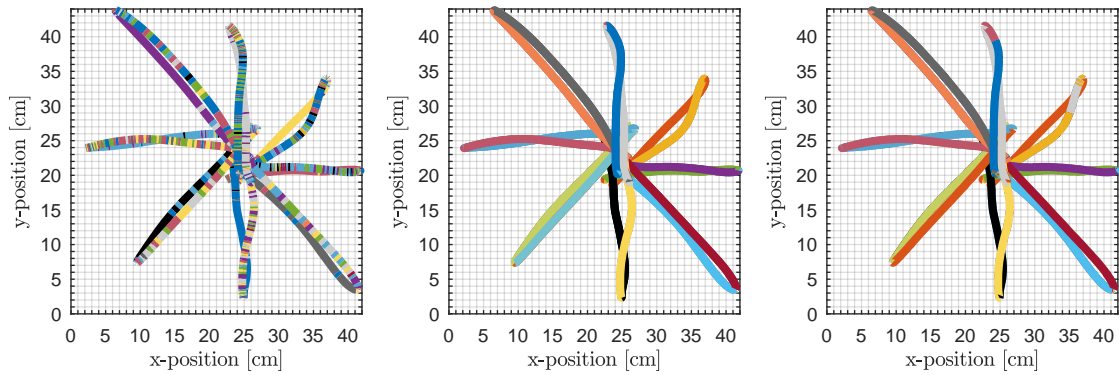


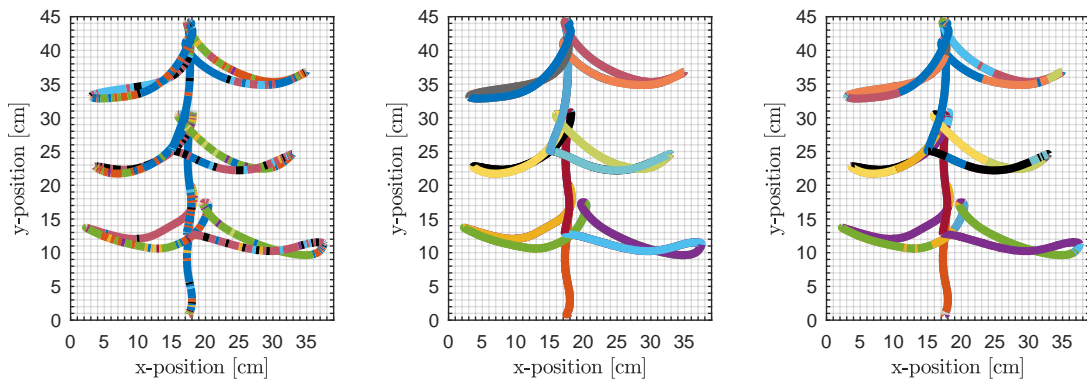
Figure 13 (continued): Motion sequences with few trajectory crossings, requiring a time-varying subgoal representation.



(f) Flower (Const)



(g) Flower (Var)



(h) Tree

Figure 13 (continued): Long motion sequences comprising a large number of sub-patterns with overlapping parts that can be only separated by considering the temporal context. Flower (Const): all strokes are performed with the same absolute velocity. Flower (Var): the individual strokes are performed with alternating velocity.

## References

- P. Abbeel and A. Y. Ng. Apprenticeship learning via inverse reinforcement learning. In *International Conference on Machine Learning*, page 1, 2004.
- M. Al-Emran. Hierarchical reinforcement learning: a survey. *International Journal of Computing and Digital Systems*, 4(2), 2015.
- S. V. Albrecht and P. Stone. Autonomous agents modelling other agents: a comprehensive survey and open problems. [arXiv:1709.08071 \[cs.AI\]](https://arxiv.org/abs/1709.08071), 2017.
- D. J. Aldous. *Exchangeability and Related Topics*. Springer, 1985.
- B. D. Argall, S. Chernova, M. Veloso, and B. Browning. A survey of robot learning from demonstration. *Robotics and Autonomous Systems*, 57(5):469–483, 2009.
- M. Babeş-Vroman, V. Marivate, K. Subramanian, and M. Littman. Apprenticeship learning about multiple intentions. In *International Conference on Machine Learning*, pages 897–904, 2011.
- L. C. Baird. Advantage updating. Technical report, Wright Lab, 1993.
- S. Bhatnagar, R. Sutton, M. Ghavamzadeh, and M. Lee. Natural actor-critic algorithms. *Automatica*, 45(11), 2009.
- D. M. Blei and P. I. Frazier. Distance dependent Chinese restaurant processes. *Journal of Machine Learning Research*, 12(Nov):2461–2488, 2011.
- D. M. Blei, A. Y. Ng, and M. I. Jordan. Latent Dirichlet allocation. *Journal of Machine Learning Research*, 3(Jan):993–1022, 2003.
- M. M. Botvinick. Hierarchical reinforcement learning and decision making. *Current Opinion in Neurobiology*, 22(6):956–962, 2012.
- S. J. Bradtke and M. O. Duff. Reinforcement learning methods for continuous-time Markov decision problems. In *Advances in Neural Information Processing Systems*, pages 393–400, 1994.
- N. Cesa-Bianchi, C. Gentile, G. Neu, and G. Lugosi. Boltzmann exploration done right. In *Advances in Neural Information Processing Systems*, pages 6275–6284, 2017.
- J. Choi and K.-E. Kim. Nonparametric Bayesian inverse reinforcement learning for multiple reward functions. In *Advances in Neural Information Processing Systems*, pages 305–313, 2012.
- C. Daniel, H. Van Hoof, J. Peters, and G. Neumann. Probabilistic inference for determining options in reinforcement learning. *Machine Learning*, 104(2-3):337–357, 2016.
- C. Dimitrakakis and C. A. Rothkopf. Bayesian multitask inverse reinforcement learning. In *European Workshop on Reinforcement Learning*, pages 273–284, 2011.

- N. J. Foti and S. A. Williamson. A survey of non-exchangeable priors for Bayesian non-parametric models. *IEEE Transactions on Pattern Analysis and Machine Intelligence*, 37(2):359–371, 2015.
- M. Ghavamzadeh, S. Mannor, J. Pineau, and A. Tamar. Bayesian reinforcement learning: a survey. *Foundations and Trends in Machine Learning*, 8(5-6):359–483, 2015.
- B. M. Kapron, V. King, and B. Mountjoy. Dynamic graph connectivity in polylogarithmic worst case time. In *Annual ACM-SIAM Symposium on Discrete Algorithms*, pages 1131–1142, 2013.
- S. Kirkpatrick, C. D. Gelatt, and M. P. Vecchi. Optimization by simulated annealing. *Science*, 220(4598):671–680, 1983.
- D. Koller and N. Friedman. *Probabilistic Graphical Models: Principles and Techniques*. MIT Press, 2009.
- G. Konidaris, S. Kuindersma, R. Grupen, and A. Barto. Robot learning from demonstration by constructing skill trees. *International Journal of Robotics Research*, 31(3):360–375, 2012.
- S. Krishnan, A. Garg, R. Liaw, L. Miller, F. T. Pokorny, and K. Goldberg. HIRL: hierarchical inverse reinforcement learning for long-horizon tasks with delayed rewards. [arXiv:1604.06508 \[cs.R0\]](https://arxiv.org/abs/1604.06508), 2016.
- S. Levine, Z. Popovic, and V. Koltun. Nonlinear inverse reinforcement learning with Gaussian processes. In *Advances in Neural Information Processing Systems*, pages 19–27, 2011.
- R. Lioutikov, G. Neumann, G. Maeda, and J. Peters. Learning movement primitive libraries through probabilistic segmentation. *International Journal of Robotics Research*, 36(8): 879–894, 2017.
- M. L. Littman, T. L. Dean, and L. P. Kaelbling. On the complexity of solving Markov decision problems. In *Conference on Uncertainty in Artificial Intelligence*, pages 394–402, 1995.
- B. Michini and J. P. How. Bayesian nonparametric inverse reinforcement learning. In *Joint European Conference on Machine Learning and Knowledge Discovery in Databases*, pages 148–163, 2012.
- B. Michini, M. Cutler, and J. P. How. Scalable reward learning from demonstration. In *IEEE International Conference on Robotics and Automation*, pages 303–308, 2013.
- B. Michini, T. J. Walsh, A.-A. Agha-Mohammadi, and J. P. How. Bayesian nonparametric reward learning from demonstration. *IEEE Transactions on Robotics*, 31(2):369–386, 2015.
- G. Neu and C. Szepesvári. Apprenticeship learning using inverse reinforcement learning and gradient methods. In *Conference on Uncertainty in Artificial Intelligence*, pages 295–302, 2007.

- A. Y. Ng and S. J. Russell. Algorithms for inverse reinforcement learning. In *International Conference on Machine Learning*, pages 663–670, 2000.
- A. Y. Ng, D. Harada, and S. Russell. Policy invariance under reward transformations: Theory and application to reward shaping. In *International Conference on Machine Learning*, pages 278–287, 1999.
- Q. P. Nguyen, B. K. H. Low, and P. Jaillet. Inverse reinforcement learning with locally consistent reward functions. In *Advances in Neural Information Processing Systems*, pages 1747–1755, 2015.
- S. Niekum, S. Osentoski, G. Konidaris, and A. G. Barto. Learning and generalization of complex tasks from unstructured demonstrations. In *IEEE/RSJ International Conference on Intelligent Robots and Systems*, pages 5239–5246, 2012.
- A. Panella and P. Gmytrasiewicz. Interactive POMDPs with finite-state models of other agents. *Autonomous Agents and Multi-Agent Systems*, pages 861–904, 2017.
- M. L. Puterman. *Markov Decision Processes: Discrete Stochastic Dynamic Programming*. John Wiley & Sons, Inc., 1994.
- D. Ramachandran and E. Amir. Bayesian inverse reinforcement learning. *International Joint Conference on Artificial Intelligence*, pages 2586–2591, 2007.
- P. Ranchod, B. Rosman, and G. Konidaris. Nonparametric Bayesian reward segmentation for skill discovery using inverse reinforcement learning. In *IEEE/RSJ International Conference on Intelligent Robots and Systems*, pages 471–477, 2015.
- G. O. Roberts and S. K. Sahu. Updating schemes, correlation structure, blocking and parameterization for the Gibbs sampler. *Journal of the Royal Statistical Society: Series B (Statistical Methodology)*, 59(2):291–317, 1997.
- C. A. Rothkopf and C. Dimitrakakis. Preference elicitation and inverse reinforcement learning. In *Joint European Conference on Machine Learning and Knowledge Discovery in Databases*, pages 34–48, 2011.
- E. Rueckert, G. Neumann, M. Toussaint, and W. Maass. Learned graphical models for probabilistic planning provide a new class of movement primitives. *Frontiers in Computational Neuroscience*, 6:97, 2013.
- S. Schaal, J. Peters, J. Nakanishi, and A. Ijspeert. Learning movement primitives. *Robotics Research*, pages 561–572, 2005.
- B. Settles. Active learning literature survey. Technical report, University of Wisconsin-Madison, 2010.
- Ö Şimşek, A. P. Wolfe, and A. G. Barto. Identifying useful subgoals in reinforcement learning by local graph partitioning. In *International Conference on Machine Learning*, pages 816–823, 2005.

- A. Šošić, A. M. Zoubir, and H. Koepl. Inverse reinforcement learning via nonparametric subgoal modeling. In *AAAI Spring Symposium on Data-Efficient Reinforcement Learning*, 2018a.
- A. Šošić, A. M. Zoubir, and H. Koepl. A Bayesian approach to policy recognition and state representation learning. *IEEE Transactions on Pattern Analysis and Machine Intelligence*, arXiv:1605.01278 [stat.ML], In Press, 2018b.
- M. Stolle and D. Precup. Learning options in reinforcement learning. In *International Symposium on Abstraction, Reformulation, and Approximation*, pages 212–223, 2002.
- A. Surana and K. Srivastava. Bayesian nonparametric inverse reinforcement learning for switched markov decision processes. In *IEEE International Conference on Learning and Applications*, pages 47–54, 2014.
- R. S. Sutton and A. G. Barto. *Reinforcement Learning: An Introduction*. MIT Press, 1998.
- R. S. Sutton, D. Precup, and S. Singh. Between MDPs and semi-MDPs: a framework for temporal abstraction in reinforcement learning. *Artificial Intelligence*, 112(1):181–211, 1999.
- M. Tamassia, F. Zambetta, W. Raffe, and X. Li. Learning options for an MDP from demonstrations. In *Australasian Conference on Artificial Life and Computational Intelligence*, pages 226–242, 2015.
- H. M. Taylor and S. Karlin. *An Introduction to Stochastic Modeling*. Academic Press, 1984.
- A. Tewari and P. L. Bartlett. Optimistic linear programming gives logarithmic regret for irreducible MDPs. In *Advances in Neural Information Processing Systems*, pages 1505–1512, 2008.
- J. Yang, Y.-G. Jiang, A. G. Hauptmann, and C.-W. Ngo. Evaluating bag-of-visual-words representations in scene classification. In *International Workshop on Multimedia Information Retrieval*, pages 197–206, 2007.
- S. Zhifei and E. M. Joo. A survey of inverse reinforcement learning techniques. *International Journal of Intelligent Computing and Cybernetics*, 5(3):293–311, 2012.
- B. D. Ziebart, A. L. Maas, J. A. Bagnell, and A. K. Dey. Maximum entropy inverse reinforcement learning. In *AAAI Conference on Artificial Intelligence*, pages 1433–1438, 2008.